UNIVERSITY OF CALIFORNIA, SAN DIEGO

Modeling and Control for the Reduction of Wave Induced Motion of Ramp-Connected Ships

A thesis submitted in partial satisfaction of the requirements for the degree Master of Science

in

Engineering Science (Mechanical Engineering)

by

Joseph L Doblack

Committee in charge:

Professor Miroslav Krstic, Chair
Professor Jorge Cortes
Professor Raymond de Callafon

2011

The Thesis of Joseph Lewis Doblack is approved, and it is acceptable in quality and form for publication on microfilm and electronically:

_____

_____

_____

Chair

University of California, San Diego

2011

Dedication

I would like to dedicate this to Chelsea. Her patience with me for as long as I've known her is seemingly endless.

Table of Contents

List of Figures

List of Tables

Acknowledgements

I would like to acknowledge Professor Krstic for his support not only on this project but in endeavors outside as well.

Over the course of my stay at UCSD I have worked with a number of students jointly and separately on this work, namely with Stephen Oonk on the SimMechanics section and Halil Basturk on the AEGIR section. All previously submitted work together is cited in this text.

ABSTRACT OF THE THESIS

Modeling and Control for the Reduction of Wave Induced Motion of Ramp-Connected Ships

by

Joseph L Doblack

Master of Science in Engineering Science (Mechanical Engineering)

University of California, San Diego, 2011

Professor Miroslav Krstic, Chair

The focus of the research in this thesis is the control of a unique vehicle in development called the T-Craft. The T-Craft is a surface effect ship (SES) capable of functioning like a catamaran or an air cushion vehicle (ACV). The goal is to ultimately stabilize a ramp connecting a large medium speed roll on/roll off (LMSR) vehicle, such as an aircraft carrier, to the T-Craft. The combination of the T-Craft connected to the LMSR is called the sea base.

The system was first modeled by treating each vessel as semi-cylinder mono-hulls and simulated using SimMechanics, a rigid body mechanical toolbox available in Matlab. The ships were connected in a bow-to-stern orientation. In this setup,

extremum seeking (ES) was used to tune the ramp length and wave heading to minimize the oscillations. Significant reduction of ramp oscillation was observed.

Following tests on the SimMechanics model, a more accurate system model was produced that utilized a wave seakeeping program called AEGIR. This program produces hydrodynamic forces based upon the hull geometry and wave information inputs. In this setup, the T-Craft was modeled as a dual hull catamaran with air cushion effects added separately and the LMSR was modeled as a large mono-hull. Passive control was tested on this new system in the form of a spring damper connection between the ramp and each vessel. Additionally, backstepping was used to control the air cushion pressure in order to reduce the heave of the T-Craft in a side by side connected system. In both cases, ramp angle oscillation reduction is observed.

Chapter 1 Introduction

The T-Craft is a surface effect ship (SES), which can alternately be supported through twin hulls similar to a catamaran or through an inflatable air cushion such as a hovercraft. However, unlike traditional SES, the T-Craft will also be operational on land similar to an air cushion vehicle (ACV). As part of its operational requirements, the T-Craft will receive cargo from the LMSR and deliver it to a nearby land target while also being able to operate for longer distances at sea as necessary. Additionally, it must be able to make the cargo transfer in adverse weather conditions. Over the course of this thesis, a few common nautical terms are used to describe the motion. Figure 1.1.1 shows the motions as well as the name for the sections of a nautical vessel.

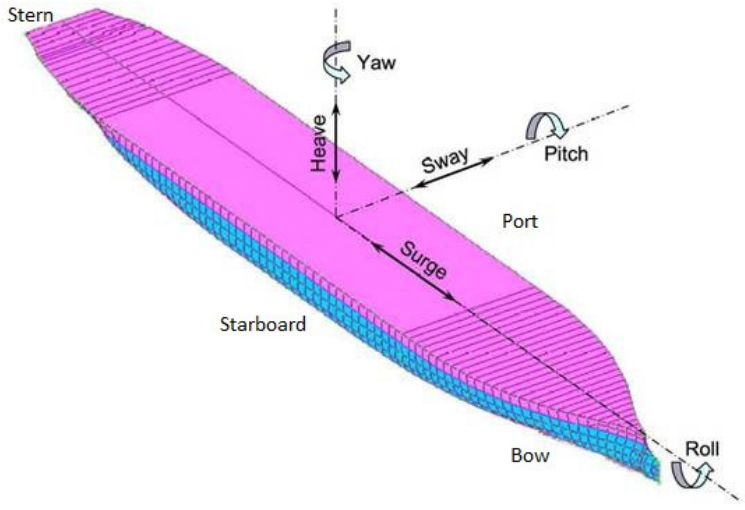

Figure 1.1.1: Nautical Terms with illustration[1]

Given the demands placed on the vessel's functionality, many elements of the T-Craft require novel design concepts. The focus of this thesis is the reduction of oscillations in the ramp during cargo transfer. Accordingly, considerable effort was made to develop a simplified yet adequate system model. For typical monohull vessels, effective equations of motion exist for the purpose of control and prediction. Creating an explicit mathematical solution to the equations of motion is difficult due to the presence of a 2nd vessel connected to the first in varying configurations.

In order to circumvent the development of the full equations of motion, the system was modeled in two ways. The first method involved using a rigid body motion solver called SimMechanics. The vessels were modeled as half cylinders connected by a ramp with hinged joints allowing the ramp to pitch with respect to the vessels. Extremum seeking was deployed to optimize the ramp length and the vessel's orientation with respect to oncoming waves.

The second method involved modeling the vessels with a naval CAD program and AEGIR, to supply the hydrodynamic forces. The forces were incorporated into the equations of motion compiled in Matlab. Passive control in the form of a spring/damper was applied to test the effectiveness on ramp oscillation. Additionally, an active control using backstepping was applied to control the air flow into the T-Craft to reduce heave and subsequently ramp oscillation.

This thesis will detail the background required into modeling each component of the system for both setups. Results and conclusions from each case are presented and discussed.

Chapter 2 SimMechanics Modeling

2.1 SimMechanics Environment

The first approach to modeling the system took place using a MATLAB toolbox called SimMechanics. SimMechanics is a rigid body dynamics solver that uses a number of block references to recreate the motion of a system. Using an approach to model ship dynamics with springs and dampers, the system can be simulated and observed in real time and allows for easier manipulation of components and settings. Additionally, SimMechanics can run using Simulink features that allow advanced control techniques. Table 2.1.1 gives a brief description for the type of block references unique to SimMechanics.

Table 2.1.1: SimMechanics environment description

Block Name	**Block description**
Machines, Bodies, Grounds	Represents rigid bodies, machines, and fixed positions at grounding points
Joints	Establishes degrees of freedom between bodies and ground points
Constraints and Drivers	Removes degrees of freedom and fixes motions between bodies
Actuators and Sensors	Applies forcing to joints or bodies and similarly records data for specified points, bodies, or joints
Force Elements	Generates the specific forcing applied to the system
Interface Elements	Interfaces three dimensional motion to one dimensional domains in Simscape
Utilities	Miscellaneous blocks for various features

The construction of a system requires care, as mistakes in the jointing and connection of vessels can cause instability during simulation. This arises not only with connections between vessels but also during actuation with respect to the global reference frame. As a result, explanation will be given not only for the joint application between the vessels but also for how the ships interact with the ground in order to simulate wave movement and allow for actuation in a desired direction.

2.2 Rigid Body Modeling

The first phase of modeling involved creating the rigid body environment in Matlab. To being with, each vessel was treated as a semi cylinder and the ramp as a rectangular box. Figure 2.2.1 illustrates a bow to stern configuration as it would be used in SimMechanics.

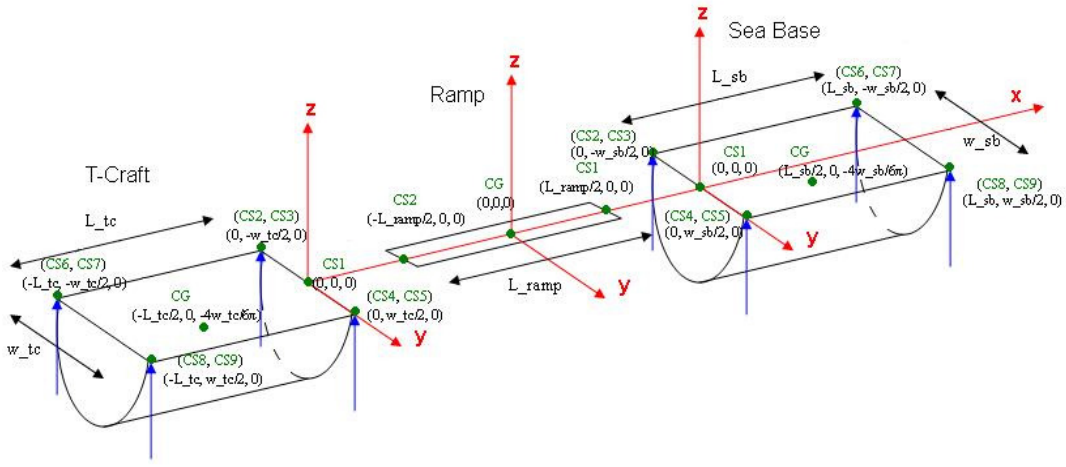

Figure 2.2.1: T-Craft and LMSR SimMechanics illustration

Though these semi cylinder bodies are not physically realistic as a true marine vessel shape, their properties are significantly simpler to calculate while still yielding adequate results. Additionally, at the first stage of system design the specifications of the T-Craft design were not available. As a result, the T-Craft was modeled as a monohull, rather than a catamaran with air cushion effects present. These discrepancies result in oscillation different from those observed from the true T-Craft. However, the control techniques applied are not model specific and as a result they can theoretically be applied in the same manner to the true system. At this stage, this model provided insight into the problem for more elaborate model synthesis and verifies the validity of controllers used in this setup. In Figure 2.2.1, red vectors indicate the axes of the Cartesian coordinate system, blue vectors indicates the wave forcing, and green points represent control points of interest, abbreviated CS, for either wave forcing or control forcing into each body.

The inertial vectors of two half cylinders and a rectangular prism are easily identified. Figures 2.2.2 and 2.2.3 show the calculations for each vector required by SimMechanics during initialization.

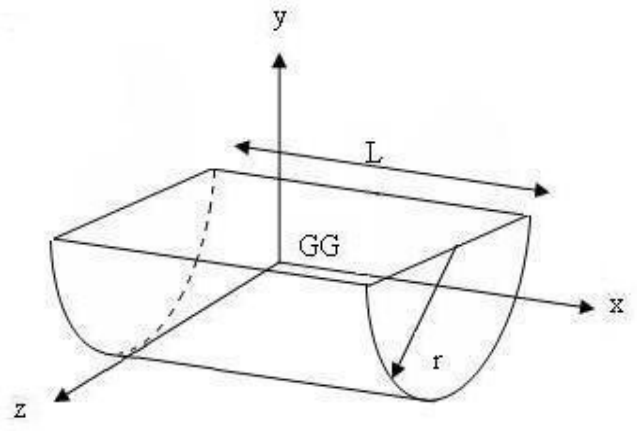

Moments of inertia through center of gravity:

$$I_{XX} = \left(\frac{1}{2} - \frac{16}{9\pi^2}\right) mr^2$$

$$I_{YY} = \frac{1}{4} mr^2 + \frac{1}{12} mL^2$$

$$I_{ZZ} = \left(\frac{1}{4} - \frac{16}{9\pi^2}\right) mr^2 + \frac{1}{12} mL^2$$

Figure 2.2.2: T-Craft and LMSR geometry and corresponding moments of inertia

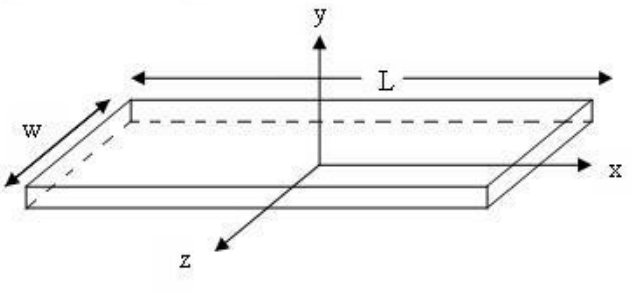

Moments of inertia through center of gravity (negligable thickness):

$$I_{XX} = \frac{1}{12} mw^2$$

$$I_{YY} = \frac{1}{4} m\left(w^2 + L^2\right)$$

$$I_{ZZ} = \frac{1}{12} mL^2$$

Figure 2.2.3: Ramp geometry and corresponding moments of inertia

All of the parameters used were selected in order to reflect realistic dimensions of the true vessels. Those parameters are listed below in table 2.2.1

Table 2.2.1: SimMechanics system parameters

Vessel/Component	**Length (m)**	**Beam (m)**	**Mass (tonne)**
LMSR	200	30	45,360
T-Craft	30	15	2720
Ramp	5	4	16

These parameters are used in the calculations regarding the rigid body properties. All the values are calculated within in Matlab and exported into SimMechanics. In addition to the mass and inertial properties, the geometry of the ships contributes to other aspects of the simulations such as formulating the equations of motions explained in further detail in the following section.

2.3 Decoupled Equations of Motion

Using the SimMechanics approach, the two vessels could be grounded to a single point with no resistance to motion from that point. The buoyant and gravity forces from the ships could then be applied in unison to produce the natural motion of the vessels at sea. While this would solve the problem of computing the equations of motion manually, there are no simple ways to calculate these forces that would require an unavailable toolbox within SimMechanics. In the absence of a hydrodynamic forcing solver, an alternative method for devising and applying the forcing from the waves was needed, namely, a method with a small number of inputs that could mimic the motion of sea vessels without requiring the full description of surface forces.

Fortunately, an approximation to standard ocean vessel motion exists using a second order mass spring and damper approach. This approach typically only applied to the heave degree of freedom, however, the method was extended to all the relevant degrees of freedom. Principally speaking, by grounding the mass of the ship with a spring and damper, a single force can be applied to each degree of freedom. By selecting an appropriate value for the stiffness and damping, this yields a periodic

motion that serves as an adequate solution to dispense with the full hydrodynamic surface forces experienced by the ship.

This method is applied to only the three relevant degrees of freedom, those being heave, pitch and roll. Surge, sway, and yaw are relatively unimportant on the oscillation of the ramp and are ignored. In practice, the vessels surge, sway, and yaw in unison and as such their effect on ramp motion is of lesser concern than primary degrees of freedom. Those motions still exist within the system and are observed in this model, but their reliance on wave motion and contribution to ramp motion is neglected. To begin, the heave motion is described by Biran $[2]$ as

$$\rho g A_w \xi \cos(\omega t) = (m + A_{33})\ddot{x}_h + b_h \dot{x}_h + \rho g A_w x_h \tag{1.1}$$

where ρ is water density, g is gravity, A_w is waterplane area, ξ is wave amplitude, ω is wave frequency (here, for a single wave input, but otherwise summing over all wave components), m is ship mass, A_{33} is the added mass, b_h is the heave damping coefficient, and x_h is the heave. The added mass term is an inertial term arising from the necessity to displace fluid during motion. This term depends on factors such as ship speed as wave characteristics and serves to reduce the overall motion of the vessel. This term can be precisely calculated dynamically at each time step; however the tools to calculate the specific values are not available. Instead, it is treated as a positive constant and added to the mass term initially. The waterplane area is the cross sectional area of the vessel at the line of contact with the water as seen in Figure 2.3.1.

While this term also varies with changing submersed portion of the vessel, it is determine by calculating the initial waterplane area at rest and keeping it constant. Biran gives no method into calculating the damping of the system; instead it is tuned in an ad hoc manner to produce reasonable results. That simply involved increasing the damping term to reduce some of the high frequency motion not present in a realistic system.

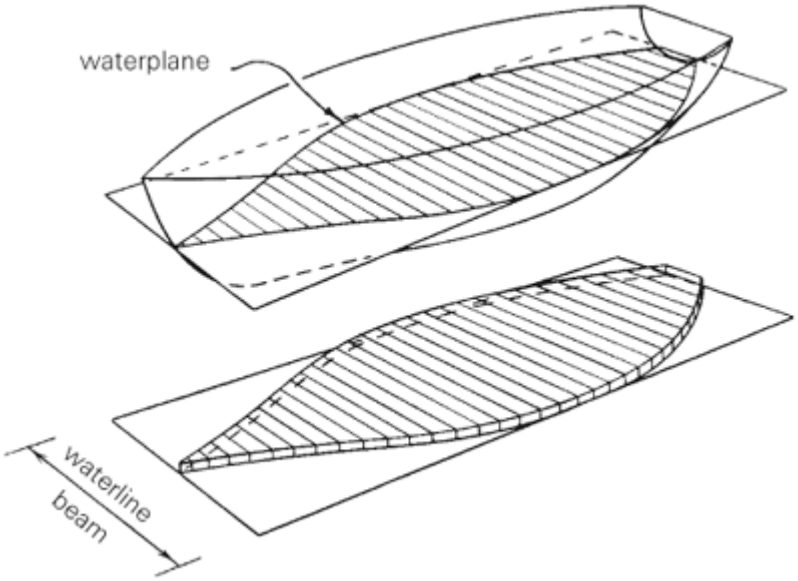

Figure 2.3.1: Illustration of waterplane area [3]

The only component that requires calculation is the waterplane area. The forcing from the waves is discussed in later sections. The waterplane area is calculated by using the favorable geometry of the semi cylindrical ship. It can be calculated abstractly since the shape of both vessels is the same with only the parameters

changing between the ships. Figure 2.3.2 shows a front view of the ship along with the terms that need to be solved.

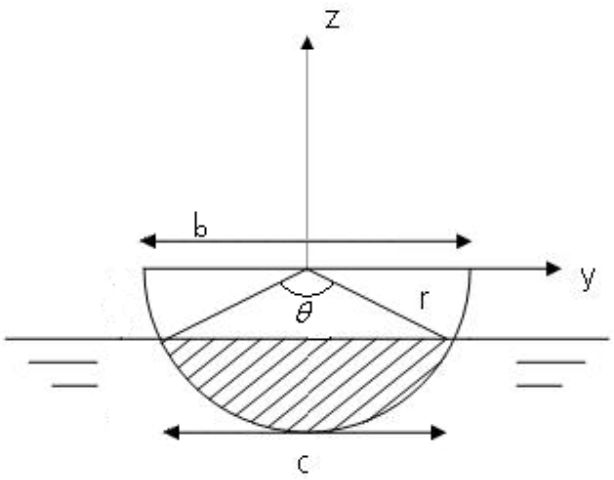

Figure 2.3.2: Terms needed to solve waterplane area

First the submersed volume is expressed in terms of ship parameters

$$V = \frac{m}{\rho} \tag{1.2}$$

where V is the submerged volume of the ship, m is the mass of the ship, and ρ is the density of water. This equals the size of the submerged segment multiplied by the ship length

$$\frac{m}{\rho} = \frac{1}{2} L\left(\theta - \sin\left(\theta\right)\right) r^2$$

$$\frac{m}{\rho} = \frac{1}{2} L\left(\theta - \sin\left(\theta\right)\right)\left(\frac{b}{2}\right)^2 \tag{1.3}$$

where θ is expressed in radians, b is the beam of the ship, and L is the length of the ship. Once θ is solved, it can be used to find c, the waterline beam.

$$\frac{1}{2}c = r\sin(\theta)$$

$$c = b\sin(\theta) \tag{1.4}$$

Finally using c to calculate waterplane area

$$A_w = Lc \tag{1.5}$$

With all of the terms calculated, the implementation into SimMechanics will be explained in more detail further on. With the heave equation of motion determined, the roll degree of freedom is considered. The uncoupled equation of motion for roll is given by

$$\omega_r^2 \xi \frac{2\pi}{\lambda}\sin(\omega t) = \ddot{x}_r + 2b_r\dot{x}_r + \omega_n^2 x_r \tag{1.6}$$

where ω_r is the ship's natural roll frequency, ω is the wave angular frequency, ξ is the wave amplitude, λ is the ocean wave length, b_r is the roll damping term, and x_r is the roll motion. The ship's natural frequency in roll, ω_n, is given by other parameters of the vessel design. Along with other important parameters, it is described by Fossen [4] as

$$\omega_r = \frac{\sqrt{gGM_R}}{i_r} \tag{1.7}$$

where GM_R is the metacentric height in roll, and i_r is the mass radius of gyration. For semi cylinders such as the ones used during simulation, the mass radius of gyration is given by

$$i_r = r\sqrt{\frac{1}{2} - \frac{16}{9\pi^2}} \approx \frac{2b}{\sqrt{3}} \tag{1.8}$$

where b is the beam of the vessel. Alternatively, it can be expressed in terms of other shape specific terms easily calculated for semi cylinders. The expression is given by

$$i_r = \frac{J_R}{\Delta} \tag{1.9}$$

where J_R is the mass moment of inertia for each ship and Δ is the volume of the displaced water. Determining the metacentric height is difficult. The metacenter is point at which the vertical lines formed from the center of buoyancy intersect when comparing the rested and a heeled position. This is more clearly illustrated in Figure 2.3.2.

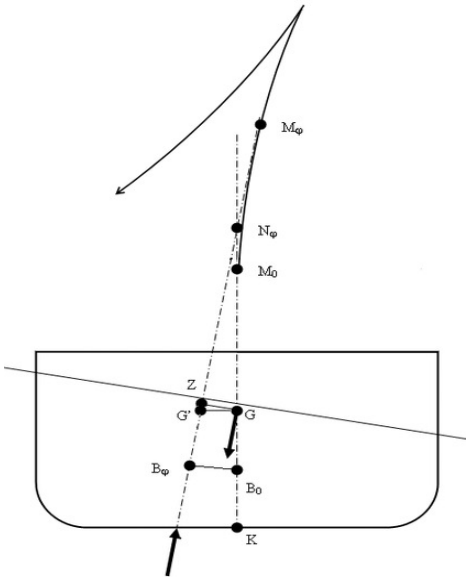

Figure 2.3.2: Illustration of metacentric height [5]

In the figure, B represents the center of buoyancy in the vessel. The center of buoyancy represents the center of mass of the displaced water and is thus located below the center of mass for the whole ship. The metacentric height represents a restoring value that helps stabilize a ship. Ships must meet a minimum metacentric height condition to be considered sea worthy. Excessively large metacentric heights result in jarring restoring forces associated with the large righting arm that attempts to restore the ship to its original position. The term is described by a sum of other geometric components of the ship and is expressed as

$$\overline{GM} = \overline{KB} + \overline{BM} - \overline{KG} \tag{1.10}$$

where K is the keel line at the base of the vessel and the other vectors are connections between the relevant points of the ship. These terms are also more easily seen in

Figure 2.3.2, where is that shows each term for a resting position and then displaced by a small angle of φ. In the figure, M is the metacenter and G is the center of gravity of the ship. Using the terms previously derived for a semi cylinder by Oonk[6], each vector is expressed as:

$$\overline{KB}_R = \frac{1}{2}b - \frac{\frac{1}{3}b^3 \sin^3\left(\cos^{-1}\left(\frac{b-2T}{b}\right)\right)}{b^2 \cos^{-1}\left(\frac{b-2T}{b}\right) - (b-4T)\sqrt{\frac{1}{4}b^2 - \left(\frac{1}{2}b - T\right)^2}} \tag{1.11}$$

$$\overline{KB}_P = \frac{1}{2}T \tag{1.12}$$

$$\overline{BM}_R = \frac{b^3}{12\left[\frac{1}{4}b^2 \cos^{-1}\left(\frac{b-2T}{b}\right) - \left(\frac{1}{2}b - T\right)\sqrt{\frac{1}{4}b^2 - \left(\frac{1}{2}b - T\right)^2}\right]} \tag{1.13}$$

$$\overline{BM}_P = \frac{bL^2}{12\left[\frac{1}{4}b^2 \cos^{-1}\left(\frac{b-2T}{b}\right) - \left(\frac{1}{2}b - T\right)\sqrt{\frac{1}{4}b^2 - \left(\frac{1}{2}b - T\right)^2}\right]} \tag{1.14}$$

$$\overline{KG}_R = b\left(\frac{1}{2} - \frac{2}{3\pi}\right) \tag{1.15}$$

$$\overline{KG}_P = b \tag{1.16}$$

Where T is the vertical distance from the waterline to the base of the ship. The subscript R represents the terms associated with the roll. The subscript P represents the

terms associated with the pitch. The metacentric height differs for each degree of freedom and is calculated separately for each. Using the terms above, the unknown values for the roll equations of motion can be solved.

The final degree of freedom considered is the pitch motion. The uncoupled equation of motion for pitch is given by

$$\omega_p^2 \xi \frac{2\pi}{\lambda} \sin(\omega t) = \ddot{x}_p + \omega_p^2 x_p \tag{1.17}$$

where ω_p is the natural frequency in pitch, ω is the angular frequency of the waves, and x_p is the pitch. The natural frequency is expressed as

$$\omega_p^2 = \frac{g\overline{GM}_P}{i_p} \tag{1.18}$$

where $\overline{GM}_P$ is the metacentric height in pitch, g is gravity, and i_p is the radius of gyration in pitch. It is calculated to be

$$i_p = \sqrt{\left(\frac{1}{16} - \frac{4}{9\pi^2}\right) b^2 + \frac{1}{12} L^2} \approx \frac{L}{2\sqrt{3}} \tag{1.19}$$

Once again the metacentric height in pitch is calculated using the previously solved terms and uncoupled equations of motions are solved in pitch, roll, and heave. The implementation and forcing term is explained in subsequent sections.

2.4 Ship-Ship and Ship-Ground connections

With the equations of motion established for the three relevant degrees of freedom, it is then necessary to implement the equations into the SimMechanics environment. The bodies interact with each other through joints inserted at specific points. In order to get the roll and pitch degrees of freedom, the forcing was modeled at the four corners of each vessel as shown in Figure 2.2.1. At each corner point, a bushing joint is placed connecting the corner to the ground. The bushing allows for translational and rotational motion in each degree of freedom. This is illustrated in Figure 2.4.1.

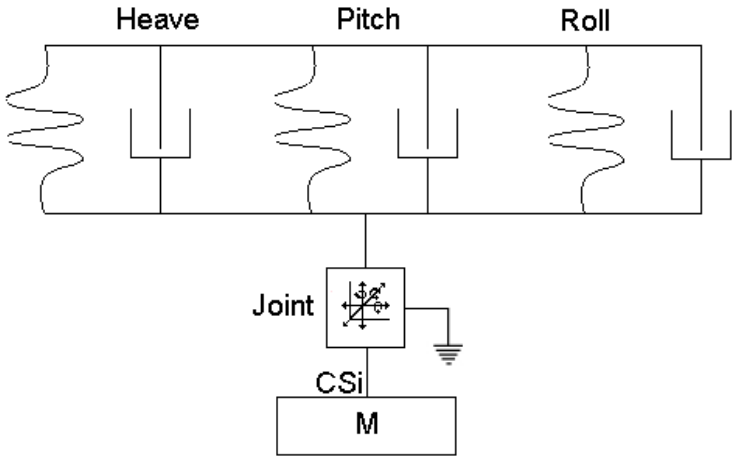

Figure 2.4.1: Spring Damper connection with vessels

The CSi point signifies the connection point specified within the mass block in SimMechanics. With each spring damper pair belonging to a specific degree of

freedom, all that remains is to define each stiffness and damping term from the equations of motion previously derived.

Once again, those equations are given as

$$\text{Heave:} \quad \rho g A_w \xi \cos(\omega t) = (m + A_{33})\ddot{x}_h + b_h \dot{x}_h + \rho g A_w x_h \tag{1.20}$$

$$\text{Pitch:} \quad \omega_p^2 \xi \frac{2\pi}{\lambda} \sin(\omega t) = \ddot{x}_p + \omega_p^2 x_p \tag{1.21}$$

$$\text{Roll:} \quad \omega_r^2 \xi \frac{2\pi}{\lambda} \sin(\omega t) = \ddot{x}_r + 2b_r \dot{x}_r + \omega_r^2 x_r \tag{1.22}$$

The equation of motion for a mass and spring damper system gives a model to fit the above equations of motion into a usable form. The equations of motion for a mass spring damper is

$$m\frac{d}{dt^2}x + c\frac{d}{dt}x + kx = F \tag{1.23}$$

Grouping the added mass term into the regular mass terms (as done internally within Matlab), the stiffness of each spring is calculated as

$$k_{heave} = \rho g A_w \tag{1.24}$$

$$k_{pitch} = \omega_p^2 m \tag{1.25}$$

$$k_{roll} = \omega_r^2 m \tag{1.26}$$

Before defining the spring constants in SimMechanics using these terms, it is important to note the differences in forcing terms. Since the forcing applied to each degree of freedom is the same within the simulation, the spring constants must be modified accordingly so the motion is appropriate for each degree of freedom. To do this, the forcing terms associated with the waves for each degree of freedom were inspected using the definitions for the natural frequency of roll and pitch. The metacentric height in roll and pitch serves as the moment arm in the equations of motion; therefore they are factored out in determining the forcing shown below

$$F_{heave} = \rho g A_w \xi \cos(\omega t) \tag{1.27}$$

$$F_{pitch} = g \triangle \xi \sin(\omega t) \tag{1.28}$$

$$F_{roll} = g \triangle \xi \sin(\omega t) \tag{1.29}$$

Separating the periodic term out leaves only the magnitudes in terms of one another. Since $\rho A_w \neq \Delta$, a normalizing term is used to ensure that the base forcing used in each degree of freedom is approximately the same. The term is simply the inverse of the heave forcing divided by the roll/pitch forcing.

$$\eta = \frac{\Delta}{\rho A_w} \tag{1.30}$$

This term is multiplied into the stiffness terms for the pitch and roll degrees of freedom to account for fact that they experience significantly less disturbance from the

waves. By reducing their stiffness, the subsequent motions modeled using the same input are equivalent to using a separate un-scaled input. With all of the terms calculated, this stiffness is simply defined within the spring box inside of SimMechanics.

Once the connection between the ships and ground are established, the two must be connected to each other. This requires some thought as to the type of connection that is required. The type of control applied to this system will require that the spacing between the ships be alterable. As such, the ramp component is broken into two separate masses allowing translation between them using a prismatic joint. The type of motion between the ramp and each ship is constrained to move in pitch only locally to the joint (roll in the global scheme). While the other types of motion might be present, their effect on the oscillation of the ramp is significantly less than the other two rotational degrees of freedom. As such, their contributions were ignored and only the pitch is considered. Figure 2.4.2 shows the connections graphically.

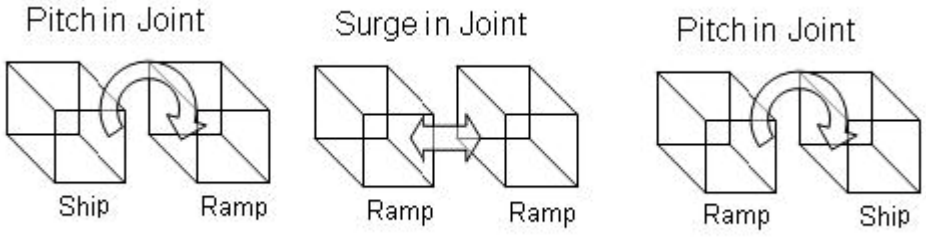

Figure 2.4.2: Ramp-ship and ramp-ramp connection

This configuration will allow the ships to move in the degrees of freedom desired while also allowing for the ramp to be extended. Moreover, this allows for the

interaction and coupled forcing to be done by SimMechanics instead of solving for the coupled equations of motion explicitly. This now completes the rigid body definitions as well as their connections to the ground and each other. The final component to complete the system is the forcing due to the waves.

2.5 Wave Modeling and Application

Ocean waves are formed through many factors and for intensive purposes are stochastic in nature. Wind generated waves occur from drag against the surface of the water that forms small waves that eventually mature into fully developed ocean waves. Waves developing in storms tend to have higher frequency components than those that are fully developed. Additionally, once the storm passes, the frequency content then shifts to a spectrum with lower frequency values. However, the simulation of developing and decaying wave patterns adds unnecessary difficulty in simulating the system. Therefore, all wave generation is done assuming fully developed conditions. Finally, some of the factors contributing to the wave generation are ignored in the dynamics of the vessels themselves. These include wind speed and ocean current that are ignored because their contribution does not affect the most pertinent states of the system. The drifting component simply moves the entire system with minimal impact to ramp motion. Wind contributes to either the surge or sway of the entire system, neither of which affects ramp oscillation.

There exist a number of wave approximation models that mimic ocean waves in a chosen environment. The method for modeling an ocean wave front typically

consists of recreating the power spectrum of wave profiles collected from empirical data. One method assumes a wave output as the result of white noise filtered through a second order filter. The output is expressed as

$$y(s) = h(s)\,w(s) \tag{1.31}$$

where $w(s)$ is the transfer function for Gaussian white noise with unity power, $\Phi_w(\omega) = 1$, and $h(s)$ is the transfer function constructed from experimental and empirical data. A model was proposed by Saelid $[7]$ as

$$h(s) = \frac{2\lambda\omega_0\sigma s}{s^2 + 2\lambda\omega_0 s + \omega_0^2} \tag{1.32}$$

where σ describes wave intensity, λ is a damping coefficient, and ω_0 is the peak frequency.

While producing an effective wave output, this method is not easily implementable in SimMechanics. This is out of necessity to vary the ships positioning with respect to the wave front. Though a wave front can be generated in advance, the variances in simulations would produce different results depending on the filtering. While the attempt is to capture the unpredictable nature of the wave, this can be done while still using a model more conducive to SimMechanics. This is done based on the principal that ocean waves can be represented as the summation of a series of sine functions

$$\zeta(x,t) = \sum_{i=1}^{N} A_i \sin(\omega_i t - k_i x + \phi_i) \tag{1.33}$$

where A is the amplitude, ω is the frequency, and ϕ is a randomly selected phase between 0 and 2π. This expression can be augmented by a noise term, again a white Gaussian signal with unity power spectrum. By choosing a single sine input with noise, the main frequency content of the wave form is preserved while some of the high frequency content is mimicked with the noise. The wave function takes the form of

$$y = A\sin(\omega t + \phi) + w \tag{1.34}$$

with A being the amplitude, ω is the dominant frequency, ϕ is a phase related to wave front distance, and w is Gaussian white noise with unity power.

From the earlier section on the uncoupled equations of motion, it is clear that it is convenient to represent the wave in terms of forcing alone. Instead of calculating lifting forces and moments, the input can be modeled by a single periodic input. From the earlier equations, it is clear that a good choice for the amplitude of this sine wave is $\rho g A_w$. The dominant frequency is chosen to represent the dominant frequency of the sea states of interest. Figure 2.5.1 shows a comparison of the second order transfer function approximation with the noisy sine wave approximation.

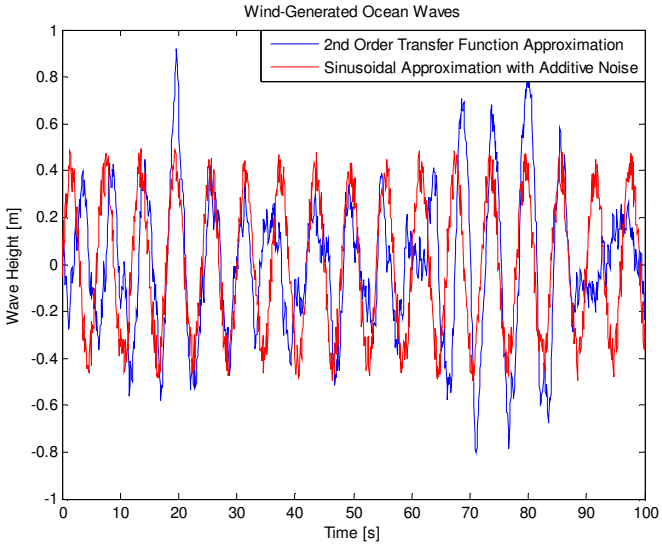

Figure 2.5.1: Filtered noise wave model vs. sinusoidal signal with noise

In the absence of a way to implement the second order filtered model, the noisy sine wave serves as an effective approximation that is easily implemented. The phase of the equation also allows for movement relative to the wave front with respect to space. Figure 2.5.2 shows the approaching wave front and the eight points of wave contact with the vessels.

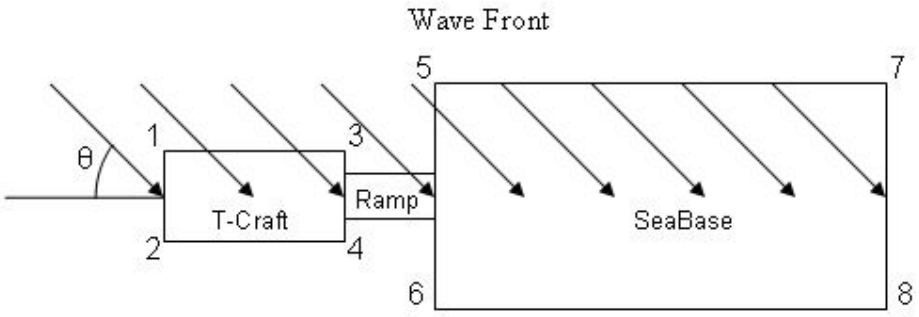

Figure 2.5.2: Sea base with wave front indicated arrows

The angle θ, the wave front angle, is used to calculate the change in phase of the wave front as the vessels move in space. Letting the phase be denoted by

$$\phi = \frac{L}{\lambda} 2\pi \tag{1.35}$$

where L is the distance from the wave front to each corner point and λ is the wavelength of the waves comprising the wave front. Figure 2.5.3 shows a top view of the system and all of the relevant parameters required to calculate the distance L needed to find the change in ϕ.

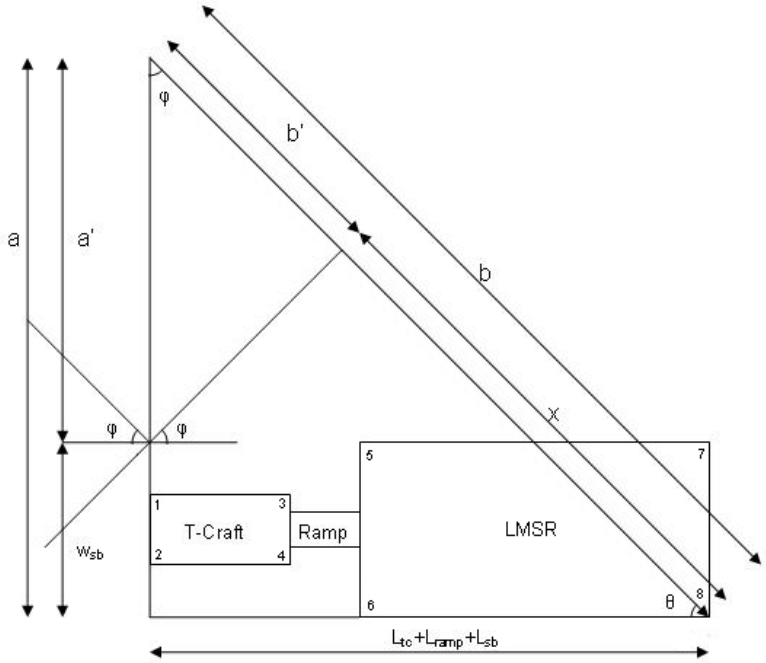

Figure 2.5.3: Wave front to control point distance calculation

Here a and b are not used explicitly, but rather to illustrate the difference in lengths between points of contact on the system. Using these parameters, Oonk [6]

geometrically solved for the distance to the wave front. His summarized values for the phase of the wave at each point is given as

Phase 1: $$\frac{\left(\frac{w_{sb}}{2}-\frac{w_{tc}}{2}\right)\sin\left(\frac{\pi}{2}-\phi\right)}{\lambda}2\pi \tag{1.36}$$

Phase 2: $$\frac{\left(w_{tc}+\frac{w_{sb}}{2}-\frac{w_{tc}}{2}\right)\sin\left(\frac{\pi}{2}-\phi\right)}{\lambda}2\pi \tag{1.37}$$

Phase 3: $$\frac{\frac{L_{tc}}{\cos\left(\frac{\pi}{2}-\phi\right)}-\left[L_{tc}\frac{\cos\phi}{\sin\phi}-\left(\frac{w_{sb}}{2}-\frac{w_{tc}}{2}\right)\right]\cos\phi}{\lambda}2\pi \tag{1.38}$$

Phase 4: $$\frac{\frac{L_{tc}}{\cos\left(\frac{\pi}{2}-\phi\right)}-\left[L_{tc}\frac{\cos\phi}{\sin\phi}-\left(w_{tc}+\frac{w_{sb}}{2}-\frac{w_{tc}}{2}\right)\right]\cos\phi}{\lambda}2\pi \tag{1.39}$$

Phase 5: $$\frac{\left(L_{tc}+L_{ramp}\right)\sin\phi}{\lambda}2\pi \tag{1.40}$$

Phase 6: $$\frac{\frac{L_{tc}+L_{ramp}}{\cos\left(\frac{\pi}{2}-\phi\right)}-\left[\left(L_{tc}+L_{ramp}\right)\frac{\cos\phi}{\sin\phi}-w_{sb}\right]\cos\phi}{\lambda}2\pi \tag{1.41}$$

Phase 7: $$\frac{\left(L_{tc}+L_{ramp}+L_{sb}\right)\sin\phi}{\lambda}2\pi \tag{1.42}$$

Phase 8: $$\frac{\dfrac{L_{tc}+L_{ramp}+L_{sb}}{\cos\left(\dfrac{\pi}{2}-\phi\right)}-\left[\left(L_{tc}+L_{ramp}+L_{sb}\right)\dfrac{\cos\phi}{\sin\phi}-w_{sb}\right]\cos\phi}{\lambda}2\pi \tag{1.43}$$

The phases are valid over the range of $\varphi\in\left(0,\frac{\pi}{2}\right]$. It should be clear from the symmetry of the system that waves approaching from $\varphi\in\left[-\frac{\pi}{2},0\right)$ are identical to the previous range of φ values. Also of note is the phase values for $\varphi=0$. To solve for these cases, L'Hopital's rule was used for the limits as $\varphi\to 0$. The results are summarized for the phase values whose denominators become 0 from Oonk [5]:

Phase 3: $$\frac{\frac{w_{sb}}{2}-\frac{w_{tc}}{2}}{\lambda}2\pi \tag{1.44}$$

Phase 4: $$\frac{w_{tc}+\frac{w_{sb}}{2}-\frac{w_{tc}}{2}}{\lambda}2\pi \tag{1.45}$$

Phase 6: $$\frac{w_{sb}}{\lambda}2\pi \tag{1.46}$$

Phase 8: $$\frac{w_{sb}}{\lambda}2\pi \tag{1.47}$$

Using these phase values, the forcing from the waves is calculated and applied to the control points at each corner of the ship. As the orientation and distances between the ships change, the phase values change accordingly and the forcing is continuously updated. This concludes the modeling section of the system in SimMechanics.

2.6 Interfacing

Since SimMechanics operates within the Simulink environment, the different components of a simulation can be addressed modularly. As a result, each aspect of the system has been explained in detail with an overview present of the model interactions and various forcing components. Figure 2.6.1 shows the communication and data flow through the system.

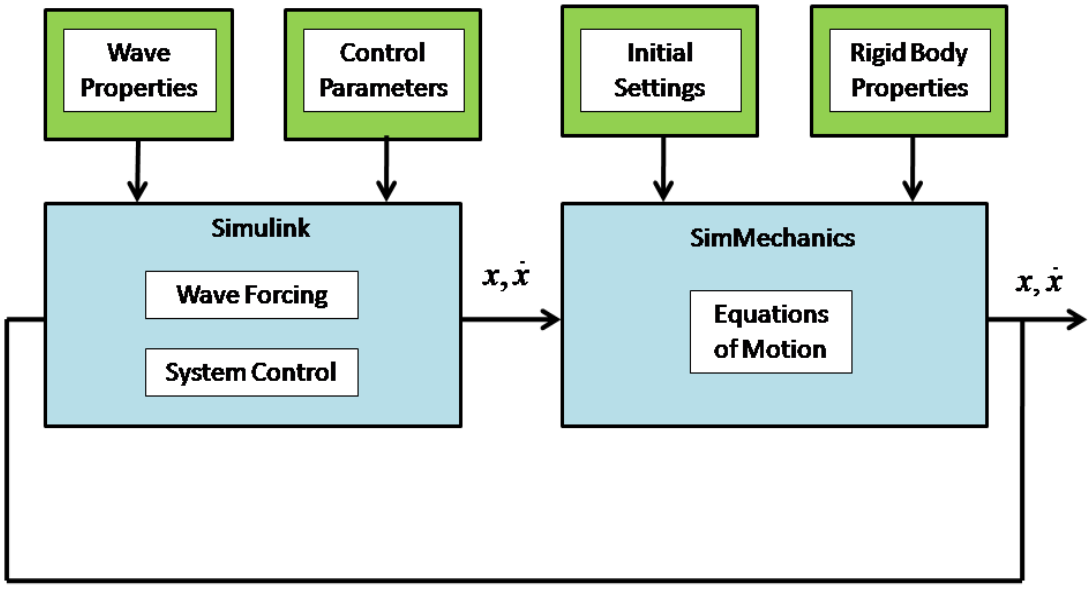

Figure 2.6.1: Interfacing information flow chart

All of the static parameters are calculated within a Matlab script that then opens the SimMechanics model. The Model includes object properties of each vessel as well as their positioning. The wave model then uses the positions of the vessels and calculates the force to apply at the various control points. Simultaneously, the controller takes the necessary states of the system and applies a positional. The process is repeated at each time step and data is collected and stored from various sensors. The simulation runs for a prescribed period then closes. There are some limitations, namely that once the properties are set in SimMechanics they can't be altered to allow for things such as mass transfer, however this platform allows enough freedom to generate an approximate sea vessel motion and still apply advanced control techniques.

Chapter 3 SimMechanics system control

Before discussing the specific controller used on this model, it is worth mentioning the limitations of the system setup to this point. Since the T-Craft is modeled primarily as a monohull in SimMechanics, there was little to no available control input into the vessel. Instead, a method was sought that would alter other factors in the system to minimize oscillations. Furthermore, without explicit model dynamics a non model based approach was considered optimal.

3.1 Extremum Seeking

With these restrictions in mind, extremum seeking was used as a controller. Extremum seeking (ES) is a powerful tool used to optimize parameters of a non-linear system around a local minimum or maximum [8]. Figure 3.1.1 shows the simplest one parameter extremum seeking loop. It uses a sinusoidal perturbation to extract gradient information and drive a system toward a local maximum or minimum.

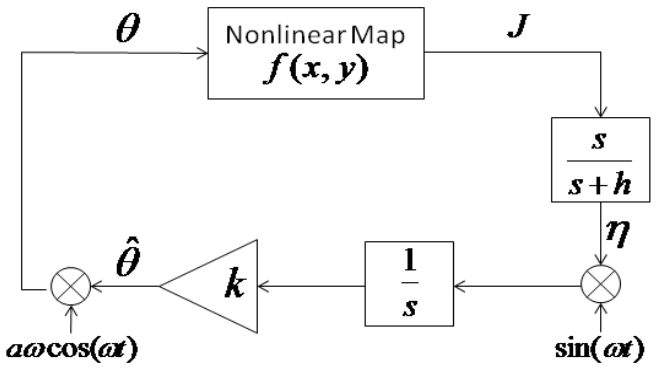

Figure 3.1.1: Standard single parameter ES loop

In this system, a two parameter extremum seeking loop is used to vary the ramp length and wave front angle independently in order to find a configuration where the oscillations are minimized. To accomplish this, the pitch angle amplitude of the ramp is used in a cost function along with the ramp length to produce a three dimensional cost plot. Due to the complex interactions between the vessels and wave forcing, the ideal values of each parameter are not obvious and instead the loop will seek out each value from a given starting position. Among the good qualities of extremum seeking is its ease of implementation. Within the Simulink environment, it merely requires the tuning of the loop parameters once the loop components are placed.

There are a couple of important points specific to this problem. Since the pitch angle signal is oscillatory with a largely static amplitude for set parameters, the signal must first be filtered to extract the overall amplitude while still allowing some of the periodic content to be present within the signal. This is done by sending the ramp pitch angle, θ, into the high pass filter $\frac{s}{s+.5}$, then squaring the value before sending into the low pass filter $\frac{1}{s+.5}$. This serves to extract the amplitude from a periodic signal but with the values of the filters chosen to preserve a small portion of the oscillations used for the loop seeking.

Additionally, since the ramp length cannot vary significantly with high frequency content, the output of the loop is filtered to include the low frequency component of the seeking signal and the final perturbation signal is omitted. These

changes are shown in Figure 3.1.2 for the modified two parameter extremum seeking loop.

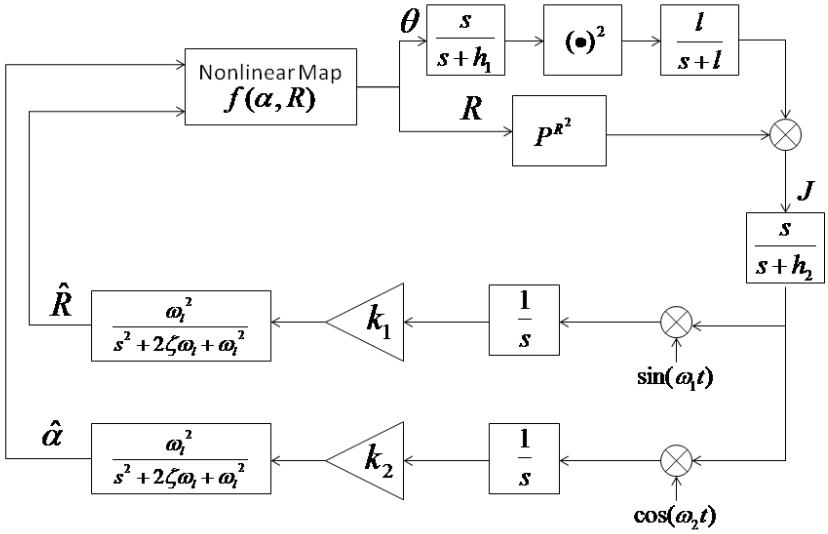

Figure 3.1.2: Modified dual parameter ES loop

where $P = 1.003$, $h_1 = .02$, $h_1 = 10$, $l = 1$, $\omega_1 = \omega_2 = 1.04$, $\omega_i = .01$, $k_1 = -1$, $k_2 = -.09$, and $\zeta = 30$. The cost, J, is formulated from multiplying the extracted pitch amplitude by a penalty on the ramp length to prevent the ramp from extending indefinitely for marginal gain. A cost map is formed by fixing each parameter over a range of values and calculating the averaged value for J over the simulation period. Figure 3.1.3 shows this completed process for ramp values of 5 to 20 meters and wave front angles of 0 to 90 degrees. The figure is displayed in log scale of the cost function to more clearly display the results.

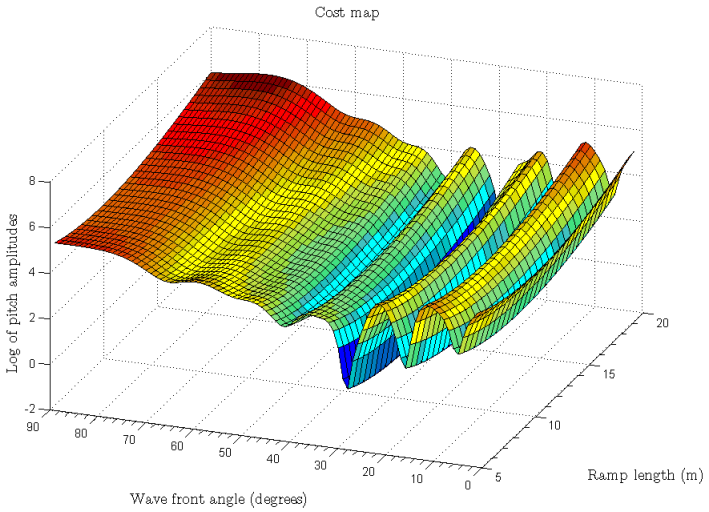

Figure 3.1.3: Cost map for wave front angle vs. ramp length

The output of the controller specifies the desired ramp length and wave front angle to minimize the cost. At each time step the positions of the ships are changed with the wave forcing updated accordingly. The system runs for a period of time allowing the loop to seek out the minimum over the domain. The results of the system simulations as well as the effects of the controller are shown in chapter 4.

Chapter 4 SimMechanics Model Results

4.1 Extremum Seeking Results

In this section results for extremum seeking used to tune ramp length and wave heading angle are presented. The system results for initial ramp length of 5 meters, with initial wave heading angles of 60° and 15°, are presented. The system is discussed in terms of wave heading angle by comparing the heave, pitch, and roll of the T-Craft for initial wave heading angles of 0° and 90° with a ramp length of 5 meters. The results from the extremum seeking are compared against a cost map. Finally, the effects of the extremum seeking are studied by analyzing the heave of the T-Craft and the ramp pitch angle.

To begin, the system is studied by considered the extreme cases of a 0° wave heading angle (directly into the bow) and a 90° wave heading angle (directly into the starboard). Wave heading is abbreviated to WH and sea state is abbreviated to SS in the figures. Figure 4.1.1 shows the heave comparison of the system for the two wave angles discussed.

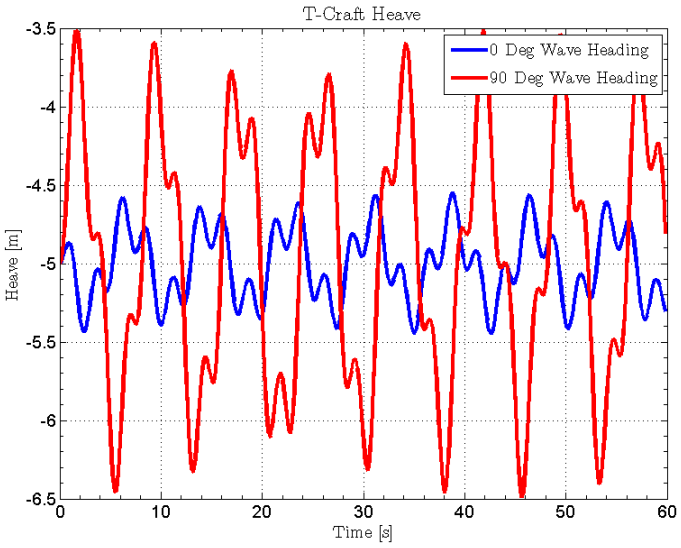

Figure 4.1.1: T-Craft Heave -SS4 WH 0, 90 Deg

Figure 4.1.2 and Figure 4.1.3 similarly show the roll and pitch for the T-Craft in the same wave heading angles.

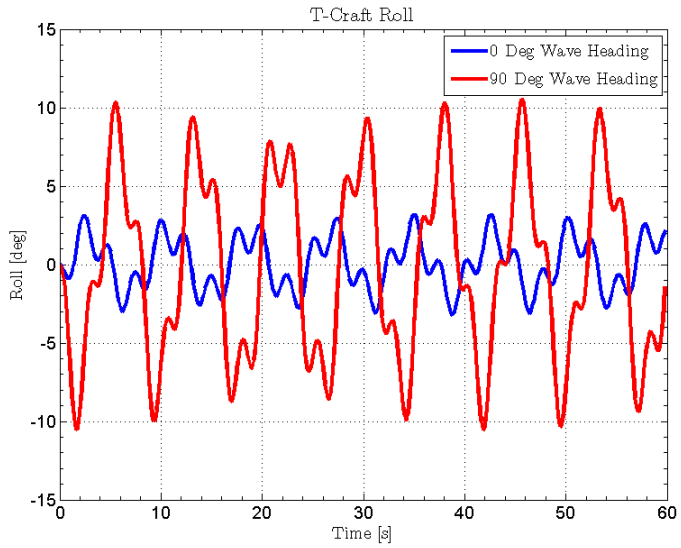

Figure 4.1.2: T-Craft Roll -SS4 WH 0, 90 Deg

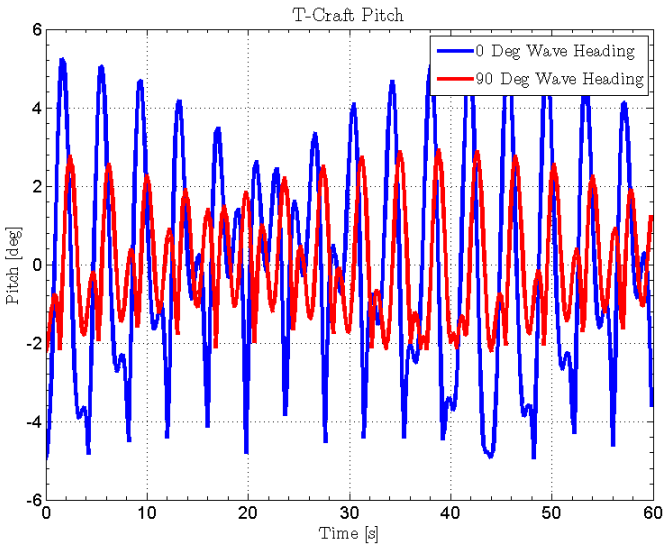

Figure 4.1.3: T-Craft Pitch -SS4 WH 0, 90 Deg

In all three of the cases it is apparent that there are two main modes in each of the degrees of freedom. This isn't surprising as the equations of motions were derived for the decoupled case. When coupled, the two masses form two dominant modes. Since the wave frequency is of a single dominant frequency, there are only two dominant visible modes. As expected the pitch is larger when approaching from the bow and the roll is maximized when approaching from the starboard. Furthermore, the difference in heave illustrates an unexpected effect when varying wave heading angle.

Figure 4.1.4 and Figure 4.1.5 show the expected minima for this system.

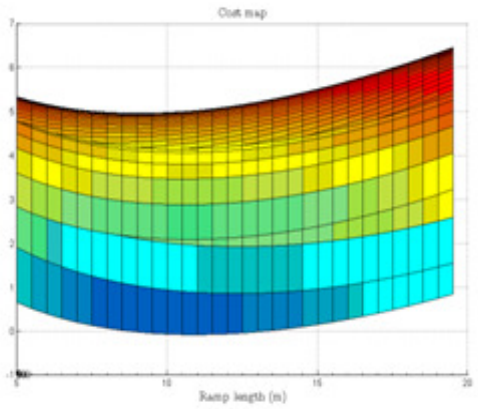

Figure 4.1.4: Cost Map Showing Ramp Optimum

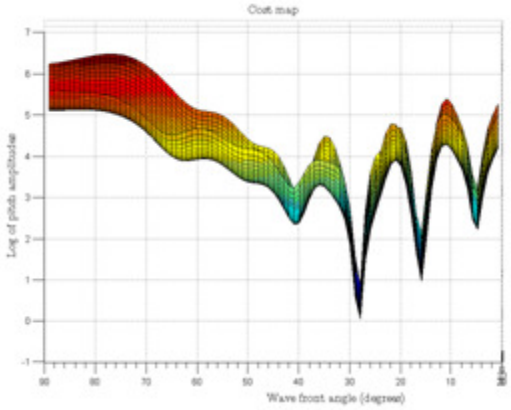

Figure 4.1.5: Cost Map Showing Wave Heading Optimum

These cost maps show us optimums the algorithm should seek. The penalty on the ramp creates a minimum visible in Figure 4.1.4 when the ramp reaches just over 11 meters long. Additionally, there are multiple local minima for wave heading angles of 29°, 16°, 6° visible in Figure 4.1.5. This will be a potential issue with this particular control method. Extremum seeking typically uses a larger perturbation or larger gains to break out of local minima and find the global minimum. However, this problem is limited by the maneuverability of the vessels. Since the vessels are

assumed to have a limited turning period, the gain must be kept to a reasonable number. That is apparent in the wave heading angle tuning in Figure 4.1.6, where the system tunes the wave heading angle to minimize the system cost. This is done for initial wave heading angles of 60° and 15°. The tuning is done in a reasonably slow fashion so that as the vessels orient themselves the wave heading finds a local minimum. Additionally, Figure 4.1.7 shows the ramp length tuning for the same initial wave heading angles.

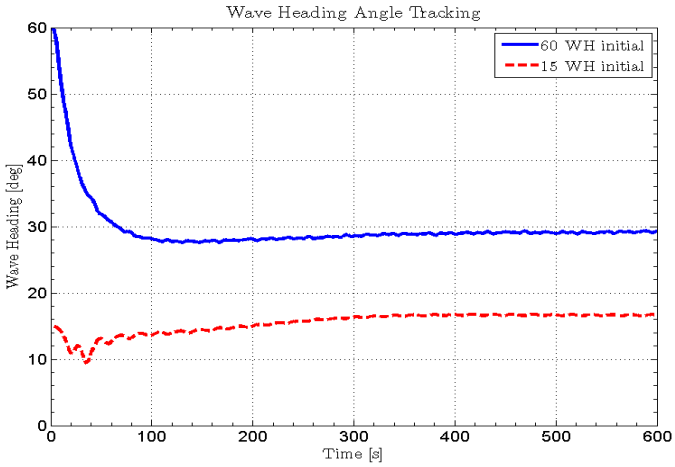

Figure 4.1.6: Extremum Seeking over Wave Heading Angle -SS4 WH 15, 60 Deg

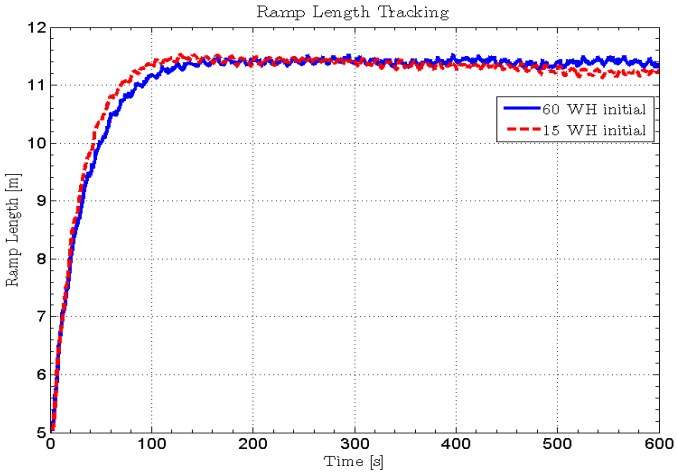

Figure 4.1.7: Extremum Seeking over Ramp Length -SS4 WH 15, 60 Deg

Both figures show successful tracking of the two parameters to local minimums. In the case of the initial wave heading angle of 60°, the ramp length tuned directly to the optimal value while maintaining that value with minimal deviation. The wave heading angle overshot slightly passed 29° but settled to it quickly. In the case of the initial wave heading angle of 15°, the wave heading angle dropped before changing directions and setting to 16°. In this variant the ramp length overshot the target initially before settling to the appropriate value and maintaining it with minimal deviation. The effect on heave is seen in Figure 4.1.8. Additionally, the effect on the ramp pitch angle is seen in Figure 4.1.9.

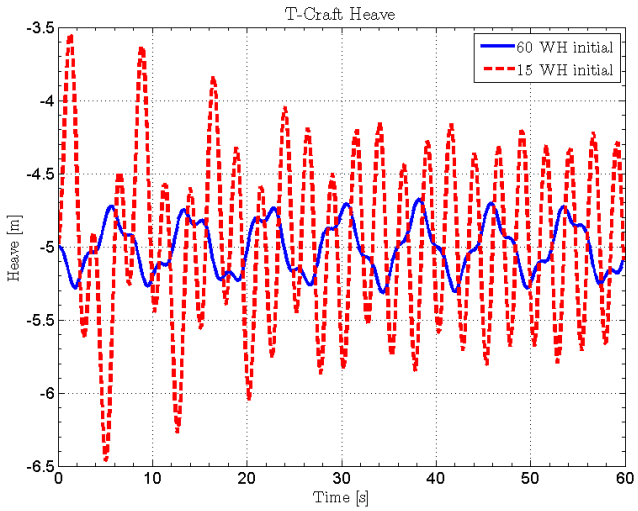

Figure 4.1.8: T-Craft Heave during seeking -SS4 WH 15, 60 Deg

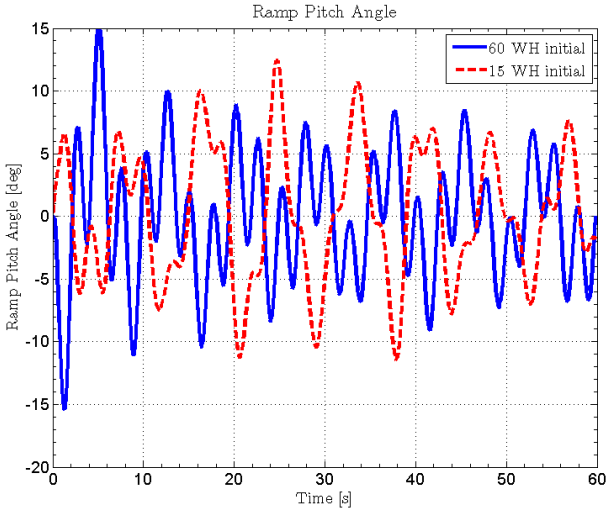

Figure 4.1.9: Ramp Pitch Angle during seeking -SS4 WH 15, 60 Deg

Figure 4.1.8 shows the increase in heave for the initial wave heading angle of 15° when the T-Craft goes to a less favorable wave heading angle before going back to a favorable angle. Once the T-Craft settles back into the local minimum the loop maintains that value. Conversely, from an initial wave heading angle of 60°, the wave heading angle and ramp nearly uniformly approach the global minimum. This is observed in Figure 4.1.8 where the heave decreases until the minimum is reached. In Figure 4.1.9 the ramp angle for each initial condition is presented. During the seek the ramp angle for the initial wave heading angle of 15° increases while the loops goes in the incorrect direction. Once it corrects and finds the local minimum, the ramp angle goes from an initial pitch angle of just over $\pm 7^{\circ}$, up to $\pm 11^{\circ}$, back to just under $\pm 7^{\circ}$. For the initial wave heading angle of 60°, the ramp pitch angle decreases almost monotonically from $\pm 15^{\circ}$ all the way down to $\pm 6^{\circ}$.

These cases show both the success and potential shortcoming of this method. While the loop will seek the local minimum regardless of initial wave angle angle, it is possible that it misses the global minimum. This is because the gain is limited and the output filtered to produce a "gentle" seek. There are potential solutions, namely starting in a favorable position such that the global minimum will be sought and maintained. This could be done by starting approaching the waves given this cost map.

Finally, after review it was decided that the ramp length would be chose initially and it would remain constant. As such, seeking over both parameters was rendered unnecessary. However, this remains an effective way to seek out optimal wave heading angles when such an application is required.

Chapter 5 AEGIR Based Modeling

The following section presents the results of the second phase of research. In this section the model using SimMechanics was discarded in favor of building the system around a wave seakeeping program called Aegir. This allowed much more realistic results including better ship models, wave models, and wave forcing. This modeling effort required many separate components explained in detail.

5.1 AEGIR Environment

The need for a higher accuracy simulation model required more advanced tools for simulating this system. Specifically, the previous model used a very simplified application of the wave hydrodynamics and their effects on the vessels. Calculation of the interaction dynamics between rigid bodies and waves for partly emerged ship hulls in turbulent sea states is a complex and challenging task. Solving and implementing these hydrodynamics would beyond the scope of our expertise. Fortunately, the development of tools to solve these problems is an active area of focus for ocean engineers. Furthermore, the increase in computing powers allows the calculations of these forces and wave deformations to be done on a single personal computer. For simulations within this thesis, the hydrodynamic time domain seakeeping tool, AEGIR, was used. AEGIR was developed at MIT's Department of Ocean Engineering and MIT's Research Lab of Electronics in 1998. It is a time-domain seakeeping code that uses an advanced, high-order boundary element method (BEM) to solve the three-

dimensional, potential-flow, and wave flow problems. Among the many features added since the first release was an overhaul of the geometry engine that allowed users to import their own CAD models for simulation. The program now automatically calculates the water line intersection to determine the wetted and dry surface areas as the vessel moves through waves.

In order to utilize the program, the user needs to define a set of parameters as well provide user vessel models and wave specifications. The details of wave production and ship modeling are provided in subsequent sections.

5.2 Rigid Body Modeling

AEGIR requires that the vessels be modeled using a popular naval CAD program called Rhino. This CAD program creates curves and surfaces using non-uniform rational basis splines (NURBS). Splines were originally created with wooden strips guided through control points intended to create curves with the reduction of the internal energy of the wood determining the curvature and shape. These wooden splines have been replaced with piecewise polynomial functions that produce curves with the added benefit of allowing designers to easily manipulate control points as well as the order of the curve polynomial.

A spline is constructed as follows. We define the spline, S, by evaluating the function, F, along points on the interval $[a,b]$ mapped to $\mathbb{R}$

$$F:[a,b]\to\mathbb{R}$$

Furthermore, $[a,b]$ can be divided into k intervals $[t_i, t_{i+1}]$ such that

$a = t_0 \le t_1 \le ..... \le t_{k-1} \le t_k = b$ for $i = 0,1,...,k-1,k$

For each of these intervals, a polynomial function, P_i, can be defined. The evaluation of these functions over each interval defines the spline.

$$S = F(t) = \begin{cases} P_o(t), & t_0 \le t \le t_1 \\ P_1(t), & t_1 \le t \le t_2 \\ \vdots & \\ P_{k-1}(t), & t_{k-1} \le t \le t_k \end{cases}$$

Among the first to use these splines for practical purposes was Pierre Bezier, after whom Bezier curves are named. He constructed a series of algorithms that produce curves based on the control points and desired order of the polynomial functions. The simplest of these is a 1st order polynomial between two points

$$B(t) = P_0 + t(P_1 - P_0), \ t \in [0,1]$$

This is simply a linear interpolation between two controls points, P_0 and P_1. Extended to a 2nd order polynomial yields

$$B(t) = (1-t)^2 P_0 + 2(1-t)tP_1 + t^2 P_2, \ t \in [0,1] \qquad (5.1)$$

This creates a quadratic function passing through control points P_0 and P_2 with P_1 having an influence on the direction of the quadratic between those points. This serves as the basis for creating an outline of the surface used in simulations.

As stated, control points are weighted data points that guide a curve or surface depending on the location of those points. In addition to control points, knot vectors contain vital information for the mapping of control points. The knot vector contains the same number of elements as the control points on a curve plus the order of the function used to fit the curve. The emphasis on knot vectors is a key difference between standard uniform Bezier curves and NURBS. Bezier curves can be expanded to three dimensional surfaces called Bezier surfaces. However, they vary from NURBS surfaces in that the knot vectors within the surfaces are not necessarily uniform as in the case of a Bezier surface. Adding a knot to a curve doesn't change the shape of the curve, it merely changes the weighting assigned to a specific control point while activating and deactivating assigned control points associated with the curve. The addition of these non-uniformly spaced knots complicated the generation of the curves, but allows greater freedom in their manipulation as well. Figure 5.2.1 illustrates a NURBS curves with Figure 5.2.2 showing the effect of adding an extra knot (and hence control point), between the third and fourth control point.

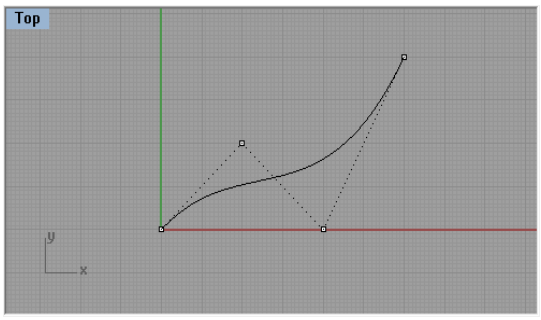

Figure 5.2.1: Uniform knot vector

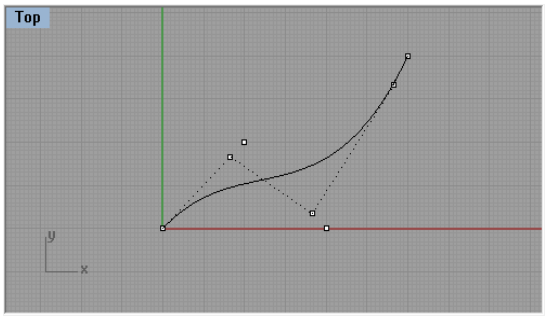

Figure 5.2.2: Added knot point

The underlying shape of the curve is maintained while the control point and knot vectors were altered. Where before the NURBS curve and Bezzier curve were identical, the added knot allows for more specific curve manipulation.

Two dimensional Bezier curves were used to generate control points that were subsequently used to generate a NURBS surface compatible with AEGIR. Using a series of Bezier curves, a skeletal frame was formed that outlined the basic structures used for simulations. The outside edges were created using dimensions mirroring realistic hull sizes for both the LMSR and T-Craft. This was done along the XZ and YZ planes as shown in Figure 5.2.3.

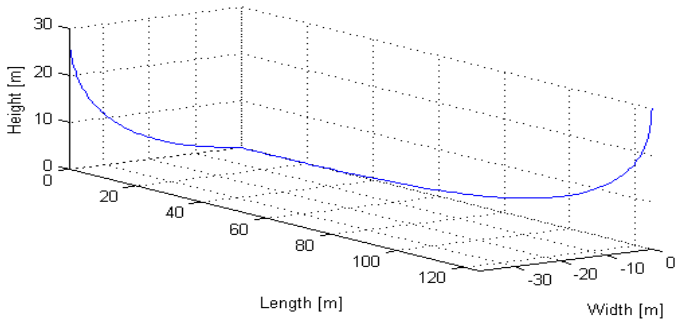

Figure 5.2.3: Bezier curves used to form edge lines

A series of curves were then formed along the base of each vessel completing the edges. These filling curves were formed by holding the Z value constant during each time step and then using the values along each outline curve as controls points for P1 and P4 respectively with P2 and P3 selected as a scaled value of P1 and P2 chosen to create a desirable edge shape. Top down and side views are shown in Figure 5.2.4 and 5.2.5.

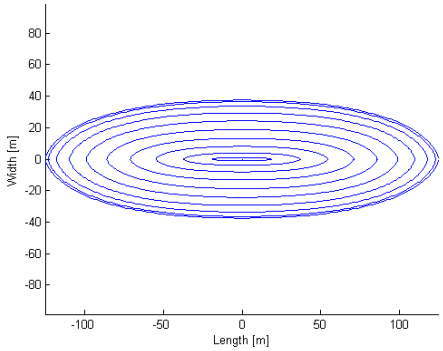

Figure 5.2.4: Top view of hull exterior

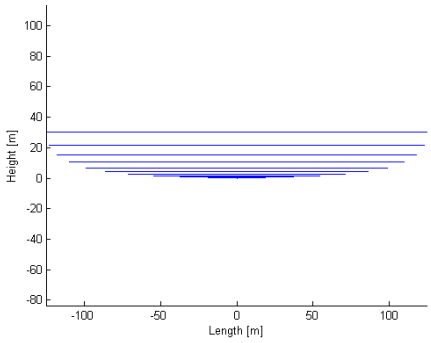

Figure 5.2.5: Side view of hull exterior

This approach allowed us to create the wigley hulls comprising a standard catamaran. A wigley hull is a term used for the specific hull type used in catamarans. It is identified by the weighting that produces its parabolic shape. The points from all the curves were collected and reordered into a single matrix. A 3rd order NURBS surface was then created using the control points along these curves with Rhino. The finished result is a two surface hull that is compatible with AEGIR. Figure 5.2.6 shows the finished surface along with the control points used in the generation process.

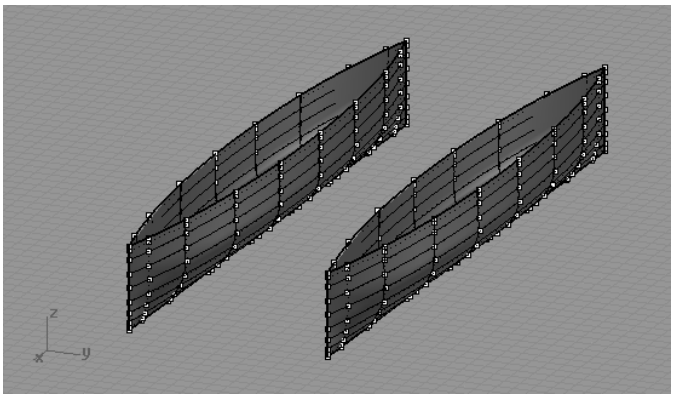

Figure 5.2.6: Rhino models for T-Craft

The T-Craft uses a flat edged dual hull system resembling a catamaran. To model these surfaces, the bow and stern edges were simply replaced by vertical lines with the port and starboard edges generated once again with Bezier curves. The LMSR was originally modeled similarly but with the curved bow and stern edges seen earlier. Though the actual LMSR shape is more refined than the one originally used, a newer LMSR cad model is now used. The effects of hull change were minor in nature due to the relative size difference between the vessels. As such, more care was given into the modeling of the T-craft as its motion was much more sensitive to the waves than the LMSR. Most importantly, the hulls were tested and found to be stable in the given ocean conditions before coupling. This is an important point as unstable models will capsize and crash simulations. Figure 5.2.7 illustrated the most recent LMSR model provided by Applied Physical Sciences used in the current simulations. Additionally, Table 5.2.1 summarizes the values of the important parameters of each vessel.

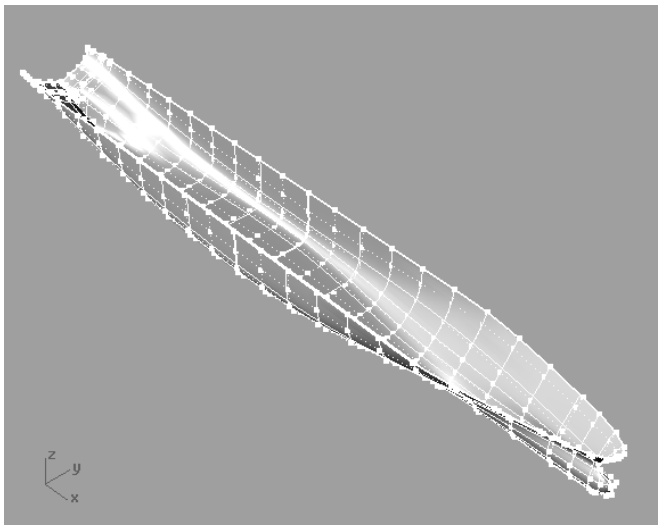

Figure 5.2.7: Rhino model for LMSR

Table 5.2.1: AEGIR environment description

Vessel/ Component	Length (m)	Beam (m)	Weight (tonnes)	Roll Radius of Gyration (m)	Pitch Radius of Gyration (m)	Yaw Radius of Gyration (m)
LMSR	301.75	76.2	81,700	12.192	60.96	60.96
T-Craft	66.2	22.86	1550	4.572	18.30	18.28
Ramp	90					

With the models completed, the ship parameters are loaded into a text file and both are then imported into AEGIR.

5.3 Air Cushion Model

This section will give detail into the effect of adding an air cushion to the catamaran model. AEGIR only provides hydrodynamic forcing for the submersed sections of the catamaran hull. As such, it is necessary to augment the model to include forces generated by an activated air cushion.

While the idea for a hovering sea vehicle had been around since the early 20th century, significant theory and designs were not rigorously tested until the 1950s. Through this phase new concepts and design led to fully functional air supported sea vessels. As their viability increased, ACVs gained attention as an option for high speed transportation to both military and commercial naval architects. This led to the increased performance in skirt design as well as the first advanced physics based models for simulating their motion. A detailed overview, by Yun and Bliault [10], summarizes much of the work done between 1950 and 2000. However, despite the amount of scientific attention it has received, there exist discrepancies between

predicted motion and experimental data. Due to the complexity of the system, such discrepancies are to be expected and improvements are still being researched.

In addition to providing the capability of high speed transportation, these ACVs have other benefits as well. The craft will be able to have a large radius of travel due to efficient fuel usage, as well as be able to transport cargo to shores. However, the most beneficial component to this project arises from the method of levitation itself. The air cushion, whose primary responsibility is to raise the craft over the water, provides a method to control the craft that would not be available otherwise. More specifically, by operating under partially inflated conditions, the air cushion allows control over the heave degree of freedom. This sort of usage is novel considering previous work into the field had been more concerned only with ride comfort. The goal is then to use the dynamics of the air cushion by changing air cushion pressure through fan and vent control that will reduce the oscillation during the cargo transfer.

The modeling involves strongly coupled effects between the air inside of the cushion, the interaction between the air and water free surface, the presence of oncoming waves, and the deformation of the skirt along with its interaction with the water. Additionally, factors such as using a partially inflated cushion as well as adding the coupling effects of the ramp makes these models incredibly difficult to implement. Instead, a simplified approach was used to model the effect of the air cushion pressure on the T-Craft.

While AEGIR provides the lifting forces associated with the rigid hulls, a separate set of equations within MATLAB provide the effect of the air cushion. This induces lifting of the craft and subsequent reduction in lifting forces provided by AEGIR. In this way both the effects of the hull and air cushion are captured simultaneously. These equations also serve as the basis for the control as they are exploited to produce the desired T-Craft displacement.

In order to derive the equations associated with air cushion, certain assumptions were made. Among them are that the contributing roll effect of the air cushion is ignored during simulations. Due to the pivotal motion of the ramp connection, their contributing effect is less severe than the heave of the body. Instead, a restoring moment is added to the system to account for uneven pressure distribution while the T-Craft is rotated. Additionally, observed phenomena such as the cobblestone effect are ignored. This particular effect arises in low sea states and causes resonant vibration in the craft due to the cushion volume change and air leakage under the specific conditions. This problem is addressed by design engineers and their contributions aren't present in the conditions tested.

To begin, Reynolds Transport Theorem $[11]$ is used for the fluid inside the air cushion

$$\frac{DB_{sys}}{Dt} = \frac{\partial}{\partial t}\int_{cv} \rho b dV + \int_{cs} \rho b V \cdot \vec{n} dA \tag{5.2}$$

where B is an extensive property of the system, mass in this system, b is an intensive property of the system, namely B per unit mass, ρ is the fluid density, V is the volume

of the system, *cv* is the control volume, *cs* is the control surface, $\vec{n}$ is the outwardly pointed normal vector to the control surface, and *A* is the area of the control surface.

The following assumptions are made for the system:

1) The hulls and skirt system comprising the air cushion are considered rigid. This results in the control volume being deformable in height only.
2) The air pressure in the air cushion is considered to be uniformly distributed.
3) The fluid in the air cushion undergoes an adiabatic process.
4) The free surface under the air cushion is considered to be rigid. This means the surface area is treated as a constant.

Mass is conserved in this system and the following continuity equation for mass is applied to the Reynolds' Transport Theorem:

$$\frac{DB_{sys}}{Dt} = \frac{\partial}{\partial t}\int_{cv} \rho b dV + \int_{cs} \rho b V \cdot \vec{n} dA \tag{5.3}$$

with $V = A_c h$ and extrapolating

$$0 = \frac{\partial}{\partial t}\int_0^h \rho A_c dh + \sum \dot{m}_{out} - \sum \dot{m}_{in}$$

$$0 = \frac{\partial}{\partial t}\left(\rho A_c h\right) + q_{out} - q_{in}$$

$$0 = \rho A_c \frac{dh}{dt} + A_c h \frac{d\rho}{dt} + q_{out} - q_{in} \tag{5.4}$$

where A_c is the cross sectional area of the air cushion, h is the height of the air cushion, $\sum \dot{m}_{out} = q_{out}$ is the mass flow rate per unit time out of the air cushion due to leakage and venting of air, and $\sum \dot{m}_{in} = q_{in}$ is the mass flow rate per unit time into the air cushion from the fans.

The air leakage out of the system, q_{out}, typically depends on a number of things including pitch and roll angles, skirt geometry, wave profile, and air cushion pressure. However, some of these factors are due to the interface between the skirt and waves at full cushion inflation. When fully inflated, the submersed portion of the skirt makes little contact with the free surface and as a result the determination of the leakage is very complex. For partially submerged hulls, the leakage is instead assumed to vary solely with pressure and not on the pressure profile as it relates to wave-skirt interactions. Therefore, q_{out} is replaced with the following term

$$q_{out} = \frac{P}{R_L} \tag{5.5}$$

where R_L is a damping term chosen to produce realistic air leakage terms out of the air cushion. The relationship is assumed to be linear inside of the operating conditions used during simulation.

The ideal gas law is then used to derive a term for the change in pressure

$$P = \frac{\rho RT}{M} \tag{5.6}$$

where R is the gas constant, T the temperature, and M the molar mass. In adiabatic processes, this equation can be expressed as

$$\frac{\partial\left(PV^{\gamma}\right)}{\partial t}=0$$

$$PV^{\gamma}=C_1$$

$$\frac{P}{\rho^{\gamma}}=C_2 \tag{5.7}$$

where C_1 and C_2 are constants and γ is the heat capacitance of the fluid. In this system, using air as the fluid the value of γ is 1.4. Now using P_0 and ρ_0 as initial values and solving for ρ with small change in pressure, $P=P_0+dP$, yields

$$\frac{P_0}{\rho_0{}^{\gamma}}=\frac{P_0+dP}{\rho^{\gamma}}$$

$$\left(\frac{\rho}{\rho_0}\right)^{\gamma}=\frac{P_0+dP}{P_0}$$

$$\rho=\rho_0\left(1+\frac{dP}{P_0}\right)^{\frac{1}{\gamma}} \tag{5.8}$$

Using a Taylor series expansion to replace the exponential yields

$$\rho = \rho_0 \left(1 + \frac{dP}{\gamma P_0} + \frac{1}{2!}\left(\frac{(\frac{1}{\gamma} - 1)}{\gamma} \right)\left(\frac{dP}{P_0} \right)^2 + \frac{1}{3!}\left(\frac{(\frac{1}{\gamma} - 1)(\frac{1}{\gamma} - 2)}{\gamma} \right)\left(\frac{dP}{P_0} \right)^3 + \ldots \right) \tag{5.9}$$

However, due to $P \gg dP$, the higher order terms of the system are ignored as

$$\left(\frac{dP}{P_0} \right)^n \approx 0 \text{ for } n \succ 1$$

Then solving for the time derivative of the expression gives

$$\frac{d\rho}{dt} = \frac{d}{dt}\rho_0 \left(1 + \frac{dP}{\gamma P_0} \right)$$

$$\frac{d\rho}{dt} = \frac{\rho_0}{\gamma P_0}\frac{dP}{dt} = \frac{\rho_0}{\gamma P_0}\dot{P} \tag{5.10}$$

Replacing this term in equation (5.4) and solving for $\dot{P}$ yields

$$\dot{P} = \frac{\gamma P_0}{A_c h \rho_0}\left(q_{in} - \frac{P}{R_L} - \rho A_c \dot{h} \right) \tag{5.11}$$

The final step is to linearize the system about initial values h_0 and ρ_0 and to simplify terms using the constant value, $C_c = \frac{\rho_0 A_c h_0}{\gamma P_0}$, that produces the final term for pressure change inside of the air cushion

$$\dot{P} = \frac{q_{in}}{C_c} - \frac{P}{C_c R_L} - \frac{\gamma P_0}{h_0}\dot{h} \tag{5.12}$$

At the beginning of the simulation all initial values are used. The pressure is divided by the air cushion footprint and applied to the equations of motion. At each time step q_{in} is determined from a control law and the change in pressure is determined with the other states of the system. Once again the force from the air cushion is calculated and applied to the equations of motion.

5.4 Equations of Motion

As described above, it was necessary to implement stand alone equations of motion in order to simulate the system using AEGIR. There are several important points that influence the derivation of these equations of motion. Firstly, AEGIR is unequipped to handle the inclusion of the ramp as an integrated component of the system. This is because the program was developed to simulate motion only for solitary vessels at sea. Any CAD models imported into the system must function only as an interactive sea vessel and therefore the ramp mass is considered to be massless. Additionally, multi hull simulations are done using mono hull models that are constrained to behave as a single vessel. Namely, the catamaran is represented by separate CAD models and thus must be treated as two masses even though their motions act as a single body. Finally, due to the connection of the LMSR and T-Craft, a Cartesian coordinate system for describing the kinetics is undesirable. Generalized

coordinates that account for the rigid connection of the two T-Craft bodies as well as the joint connection between the LMSR and T-Craft are used instead.

The first step is to establish the center of mass for the entire system. From this point, the system is allowed free motion about the intermediate frame as a single body. Allowing free motion around the center of mass allows easier implementation of the equations motion rather than using an arbitrary origin elsewhere. Secondly, the ramp connections are assumed to be fixed, disallowing any translational movement at the pivot points. This constrains motion such that no relative heave, sway, or surge is allowed. Initially, the pivot points referred to as $\vec{p}_1$ and $\vec{p}_2$ for the connection between the ramp and LMSR and ramp and T-Craft respectively, are allowed to have full rotational movement in pitch, roll, and yaw degrees of freedom. Once again the connection between the two catamarans hulls comprising the T-Craft is fully constrained so that their connection is rigid.

This initially creates a total of twelve degrees of freedom described by

$$\vec{\zeta}_T = \{\zeta_1, \zeta_2, \zeta_3\} \tag{5.13}$$

$$\vec{\zeta}_R = \{\zeta_4, \zeta_5, \zeta_6\} \tag{5.14}$$

$$\vec{\xi}_1 = \{\zeta_7, \zeta_8, \zeta_9\} \tag{5.15}$$

$$\vec{\xi}_2 = \{\zeta_{10}, \zeta_{11}, \zeta_{12}\} \tag{5.16}$$

where $\vec{\zeta}_T$ is the translational motion, $\vec{\zeta}_R$ the rotational motion of the combined 2-vehicle system about the intermediate frame of reference, $\vec{\xi}_1$ and $\vec{\xi}_2$ are the roll, pitch and yaw angles for each of the two pivot points defining their orientation relative to the averaged rotations of the whole system.

The bodies can then be expressed in a global reference frame using these generalized coordinates, with initial position $\vec{x}_0$, with the following expression $[12]$

$$\vec{x}_1(t) = \vec{\zeta}_T(t) + [T]_{\vec{\zeta}_R}(t)\vec{x}_0 + [T]_{\vec{\xi}_1}(t)(\vec{x}_0 - \vec{p}_1) \tag{5.17}$$

where $[T]$ represents the nonlinear Eulerian rotation matrix and $\vec{p}_1$ is the location of the arm pivot on the first body. This expression can be simplified for small motions by replacing the nonlinear Eulerian matrices $[12]$ with the linearized equation

$$\vec{x}_1(t) = \vec{\zeta}_T(t) + \vec{\zeta}_R(t) \times \vec{x}_0 + \vec{\xi}_1(t) \times (\vec{x}_0 - \vec{p}_1) \tag{5.18}$$

Hence the centers of mass $\vec{x}_{c_1} = \begin{pmatrix} x_{c_1} \\ y_{c_1} \\ z_{c_1} \end{pmatrix}, \vec{x}_{c_2} = \begin{pmatrix} x_{c_2} \\ y_{c_2} \\ z_{c_2} \end{pmatrix}, \vec{x}_{c_3} = \begin{pmatrix} x_{c_3} \\ y_{c_3} \\ z_{c_3} \end{pmatrix}$ of bodies one, two and three with its initial positions $\vec{x}_{c_1}^0, \vec{x}_{c_2}^0, \vec{x}_{c_3}^0$ can be expressed in a global reference frame as follows

$$\vec{x}_{c_1}(t)=\begin{pmatrix}\zeta_1\\ \zeta_2\\ \zeta_3\end{pmatrix}+\begin{pmatrix}\zeta_4\\ \zeta_5\\ \zeta_6\end{pmatrix}\times\begin{pmatrix}x_{c_1}^0\\ y_{c_1}^0\\ z_{c_1}^0\end{pmatrix}+\begin{pmatrix}\zeta_7\\ \zeta_8\\ \zeta_9\end{pmatrix}\times\begin{pmatrix}x_{c_1}^0-x_{p_1}\\ y_{c_1}^0-y_{p_1}\\ z_{c_1}^0-z_{p_1}\end{pmatrix}$$
$$=\begin{pmatrix}\zeta_1+\left(z_{c_1}^0\zeta_5-y_{c_1}^0\zeta_6\right)+\left(z_{c_1}^0-z_{p_1}\right)\zeta_8-\left(y_{c_1}^0-y_{p_1}\right)\zeta_9\\ \zeta_2+\left(x_{c_1}^0\zeta_6-z_{c_1}^0\zeta_4\right)+\left(x_{c_1}^0-x_{p_1}\right)\zeta_9-\left(z_{c_1}^0-z_{p_1}\right)\zeta_7\\ \zeta_3+\left(y_{c_1}^0\zeta_4-x_{c_1}^0\zeta_5\right)+\left(y_{c_1}^0-y_{p_1}\right)\zeta_7-\left(x_{c_1}^0-x_{p_1}\right)\zeta_8\end{pmatrix} \tag{5.19}$$

$$\vec{x}_{c_3}(t)=\begin{pmatrix}\zeta_1\\ \zeta_2\\ \zeta_3\end{pmatrix}+\begin{pmatrix}\zeta_4\\ \zeta_5\\ \zeta_6\end{pmatrix}\times\begin{pmatrix}x_{c_2}^0\\ y_{c_2}^0\\ z_{c_2}^0\end{pmatrix}+\begin{pmatrix}\zeta_{10}\\ \zeta_{11}\\ \zeta_{12}\end{pmatrix}\times\begin{pmatrix}x_{c_2}^0-x_{p_2}\\ y_{c_2}^0-y_{p_2}\\ z_{c_2}^0-z_{p_2}\end{pmatrix}$$
$$=\begin{pmatrix}\zeta_1+\left(z_{c_2}^0\zeta_5-y_{c_2}^0\zeta_6\right)+\left(z_{c_2}^0-z_{p_2}\right)\zeta_{11}-\left(y_{c_2}^0-y_{p_2}\right)\zeta_{12}\\ \zeta_2+\left(x_{c_2}^0\zeta_6-z_{c_2}^0\zeta_4\right)+\left(x_{c_2}^0-x_{p_2}\right)\zeta_{12}-\left(z_{c_2}^0-z_{p_2}\right)\zeta_{10}\\ \zeta_3+\left(y_{c_2}^0\zeta_4-x_{c_2}^0\zeta_5\right)+\left(y_{c_2}^0-y_{p_2}\right)\zeta_{13}-\left(x_{c_2}^0-x_{p2}\right)\zeta_{11}\end{pmatrix} \tag{5.20}$$

$$\vec{x}_{c_3}(t)=\begin{pmatrix}\zeta_1\\ \zeta_2\\ \zeta_3\end{pmatrix}+\begin{pmatrix}\zeta_4\\ \zeta_5\\ \zeta_6\end{pmatrix}\times\begin{pmatrix}x_{c_3}^0\\ y_{c_3}^0\\ z_{c_3}^0\end{pmatrix}+\begin{pmatrix}\zeta_{10}\\ \zeta_{11}\\ \zeta_{12}\end{pmatrix}\times\begin{pmatrix}x_{c_3}^0-x_{p_2}\\ y_{c_3}^0-y_{p_2}\\ z_{c_3}^0-z_{p_2}\end{pmatrix}$$
$$=\begin{pmatrix}\zeta_1+\left(z_{c_3}^0\zeta_5-y_{c_3}^0\zeta_6\right)+\left(z_{c_3}^0-z_{p_2}\right)\zeta_{11}-\left(y_{c_3}^0-y_{p_2}\right)\zeta_{12}\\ \zeta_2+\left(x_{c_3}^0\zeta_6-z_{c_3}^0\zeta_4\right)+\left(x_{c_3}^0-x_{p_2}\right)\zeta_{12}-\left(z_{c_3}^0-z_{p_2}\right)\zeta_{10}\\ \zeta_3+\left(y_{c_3}^0\zeta_4-x_{c_3}^0\zeta_5\right)+\left(y_{c_3}^0-y_{p_2}\right)\zeta_{10}-\left(x_{c_3}^0-x_{p2}\right)\zeta_{11}\end{pmatrix} \tag{5.21}$$

These expressions for the centers of mass in generalized coordinates can now be used to derive the equations of motions using the approach of Lagrangian Mechanics. The use of Lagrangian method simplifies the derivation of equations of motions by using the generalized coordinate system to produce naturally constrained results. Attempting to formulate the equations of motion without this method requires

much more effort and allows for more errors when constraining the motions. The Lagrange's equations are defined as [13]

$$L = T - U$$

$$\frac{d}{dt}\left(\frac{\partial L}{\partial \dot{\zeta}_j}\right) - \frac{\partial L}{\partial \zeta_j} = \Xi_j \text{ for } \quad j = 1,...,12 \tag{5.22}$$

where T is kinetic energy, U it the potential energy and Ξ_j the generalized forces and moments for each of the generalized coordinates ζ_j .

The kinetic energy, T, of the 3-body system can be expressed as a sum of kinetic energies of each of the three bodies T_1, T_2, and T_3

$$T = T_1 + T_2 + T_3 \tag{5.23}$$

For each body the kinetic energy can be expressed in terms of motion along the axis of the intermediate reference frame, combined with the rotations around the axis of body-fixed coordinate frame, with φ_b, θ_b, and ψ_b as rotation angles around its principal axis. This results in the kinetic energies being expressed as

$$T_1 = \frac{1}{2}m_1\dot{x}_1^2 + \frac{1}{2}m_1\dot{y}_1^2 + \frac{1}{2}m_1\dot{z}_1^2 + \frac{1}{2}I_{x_1}\dot{\varphi}_1^2 + \frac{1}{2}I_{y_1}\dot{\theta}_1^2 + \frac{1}{2}I_{z_1}\dot{\psi}_1^2 \tag{5.24}$$

$$T_2 = \frac{1}{2}m_2\dot{x}_2^2 + \frac{1}{2}m_2\dot{y}_2^2 + \frac{1}{2}m_2\dot{z}_2^2 + \frac{1}{2}I_{x_2}\dot{\varphi}_2^2 + \frac{1}{2}I_{y_2}\dot{\theta}_2^2 + \frac{1}{2}I_{z_2}\dot{\psi}_2^2 \tag{5.25}$$

$$T_3 = \frac{1}{2}m_3\dot{x}_3^2 + \frac{1}{2}m_3\dot{y}_3^2 + \frac{1}{2}m_3\dot{z}_3^2 + \frac{1}{2}I_{x_3}\dot{\varphi}_3^2 + \frac{1}{2}I_{y_3}\dot{\theta}_3^2 + \frac{1}{2}I_{z_3}\dot{\psi}_3^2 \tag{5.26}$$

where m_i is the mass of the body i and $I_{x_i}, I_{y_i}, I_{z_i}$ the moments of inertia about that bodies centers of gravity.

Using equations 5.24, 5.25 and 5.26, the total kinetic energy T of the of the 3-body system can be expressed in terms of generalized coordinates

$$
\begin{aligned}
T = {} & \frac{1}{2} m_1 \left[\dot{\zeta}_1 + \left(z_{c_1}^0 \dot{\zeta}_5 - y_{c_1}^0 \dot{\zeta}_6 \right) + \left(z_{c_1}^0 - z_{p_1} \right) \dot{\zeta}_8 - \left(y_{c_1}^0 - y_{p_1} \right) \dot{\zeta}_9 \right]^2 \\
& + \frac{1}{2} m_1 \left[\dot{\zeta}_2 + \left(x_{c_1}^0 \dot{\zeta}_6 - z_{c_1}^0 \dot{\zeta}_4 \right) + \left(x_{c_1}^0 - x_{p_1} \right) \dot{\zeta}_9 - \left(z_{c_1}^0 - z_{p_1} \right) \dot{\zeta}_7 \right]^2 \\
& + \frac{1}{2} m_1 \left[\dot{\zeta}_3 + \left(y_{c_1}^0 \dot{\zeta}_4 - x_{c_1}^0 \dot{\zeta}_5 \right) + \left(y_{c_1}^0 - y_{p_1} \right) \dot{\zeta}_7 - \left(x_{c_1}^0 - x_{p_1} \right) \dot{\zeta}_8 \right]^2 \\
& + \frac{1}{2} I_{x_1} \left(\dot{\zeta}_4 + \dot{\zeta}_7 \right)^2 + \frac{1}{2} I_{y_1} \left(\dot{\zeta}_5 + \dot{\zeta}_8 \right)^2 + \frac{1}{2} I_{z_1} \left(\dot{\zeta}_6 + \dot{\zeta}_9 \right)^2 \\
& + \frac{1}{2} m_2 \left[\dot{\zeta}_1 + \left(z_{c_2}^0 \dot{\zeta}_5 - y_{c_2}^0 \dot{\zeta}_6 \right) + \left(z_{c_2}^0 - z_{p_2} \right) \dot{\zeta}_{11} - \left(y_{c_2}^0 - y_{p_2} \right) \dot{\zeta}_{12} \right]^2 \\
& + \frac{1}{2} m_2 \left[\dot{\zeta}_2 + \left(x_{c_2}^0 \dot{\zeta}_6 - z_{c_2}^0 \dot{\zeta}_4 \right) + \left(x_{c_2}^0 - x_{p_2} \right) \dot{\zeta}_{12} - \left(z_{c_2}^0 - z_{p_2} \right) \dot{\zeta}_{10} \right]^2 \\
& + \frac{1}{2} m_2 \left[\dot{\zeta}_3 + \left(y_{c_2}^0 \dot{\zeta}_4 - x_{c_2}^0 \dot{\zeta}_5 \right) + \left(y_{c_2}^0 - y_{p_2} \right) \dot{\zeta}_{10} - \left(x_{c_2}^0 - x_{p_2} \right) \dot{\zeta}_{11} \right]^2 \\
& + \frac{1}{2} I_{x_2} \left(\dot{\zeta}_4 + \dot{\zeta}_{10} \right)^2 + \frac{1}{2} I_{y_2} \left(\dot{\zeta}_5 + \dot{\zeta}_{11} \right)^2 + \frac{1}{2} I_{z_2} \left(\dot{\zeta}_6 + \dot{\zeta}_{12} \right)^2 \\
& + \frac{1}{2} m_3 \left[\dot{\zeta}_1 + \left(z_{c_3}^0 \dot{\zeta}_5 - y_{c_3}^0 \dot{\zeta}_6 \right) + \left(z_{c_3}^0 - z_{p_2} \right) \dot{\zeta}_{11} - \left(y_{c_3}^0 - y_{p_2} \right) \dot{\zeta}_{12} \right]^2 \\
& + \frac{1}{2} m_3 \left[\dot{\zeta}_2 + \left(x_{c_3}^0 \dot{\zeta}_6 - z_{c_3}^0 \dot{\zeta}_4 \right) + \left(x_{c_3}^0 - x_{p_2} \right) \dot{\zeta}_{12} - \left(z_{c_3}^0 - z_{p_2} \right) \dot{\zeta}_{10} \right]^2 \\
& + \frac{1}{2} m_3 \left[\dot{\zeta}_3 + \left(y_{c_3}^0 \dot{\zeta}_4 - x_{c_3}^0 \dot{\zeta}_5 \right) + \left(y_{c_3}^0 - y_{p_2} \right) \dot{\zeta}_{10} - \left(x_{c_3}^0 - x_{p_2} \right) \dot{\zeta}_{11} \right]^2 \\
& + \frac{1}{2} I_{x_3} \left(\dot{\zeta}_4 + \dot{\zeta}_{10} \right)^2 + \frac{1}{2} I_{y_3} \left(\dot{\zeta}_5 + \dot{\zeta}_{11} \right)^2 + \frac{1}{2} I_{z_3} \left(\dot{\zeta}_6 + \dot{\zeta}_{12} \right)^2
\end{aligned}
\tag{5.27}
$$

Similarly, for the expression of potential energy in terms of generalized coordinates follows the same form as the kinetic energy, expressed as

$$
\begin{aligned}
U &= m_1 g z_1 + m_2 g z_3 + m_3 g z_3 \\
&= m_1 g \left[\zeta_3 + \left(y_{c_1}^0 \zeta_4 - x_{c_1}^0 \zeta_5 \right) + \left(y_{c_1}^0 - y_{p_1} \right) \zeta_7 - \left(x_{c_1}^0 - x_{p_1} \right) \zeta_8 \right] \\
&+ m_2 g \left[\zeta_3 + \left(y_{c_2}^0 \zeta_4 - x_{c_2}^0 \zeta_5 \right) + \left(y_{c_2}^0 - y_{p_2} \right) \zeta_{13} - \left(x_{c_2}^0 - x_{p2} \right) \zeta_{11} \right] \\
&+ m_3 g \left[\zeta_3 + \left(y_{c_3}^0 \zeta_4 - x_{c_3}^0 \zeta_5 \right) + \left(y_{c_3}^0 - y_{p_2} \right) \zeta_{10} - \left(x_{c_3}^0 - x_{p2} \right) \zeta_{11} \right]
\end{aligned}
\tag{5.28}
$$

With the terms for kinetic and potential energy formulated, the Lagrangian approach can now be used to solve for the motion of the system. However, in order to minimize computational time, the degrees of freedom of the system were constricted such that only certain motions were considered. Namely, only some of the 12 degrees of freedom were considered relevant in solving the ramp stabilization problem. Of the 3 rotational degrees of freedom at each joint, only pitch was considered. Since the yaw of the joint would only be minimal due to the parallel nature of the vessels, it is ignored for the purposes of simulation. In test craft, the joint is gimbaled to allow these small yaw motions without breaking the ramp in the presence of a rigid connection. Due to the presence of mechanism to allow their motions in the vehicle but their relative small effect on ramp motion, as well as limited methods into their suppression, their generalized coordinates are set to zero. Similarly, there is strictly no roll allowed in the ramp. In practice this is accomplished by matching speeds and relative surge positions of the vessels and is a necessary aspect of the cargo transportation. As this is an external component not relevant to the actual ramp motion, their generalized coordinates are also set to zero.

Furthermore, the six degrees of freedom of the entire 3-body system are reduced to the three relevant motions. Namely, the surge and sway motions of the

connected craft don't contribute to the oscillation of ramp. Relative differences in heave are critical to the motion of the ramp and are solely considered for the translational motion of the system. Additionally, the heading of the sea base is considered to be maintained during transfer and is therefore set to zero during simulation. Only pitch and roll are considered as there is no control possible over these rotational degrees of freedom. Figure 5.4.1 illustrates the unconstrained degrees of freedom and how each moves with respect to the global reference frame.

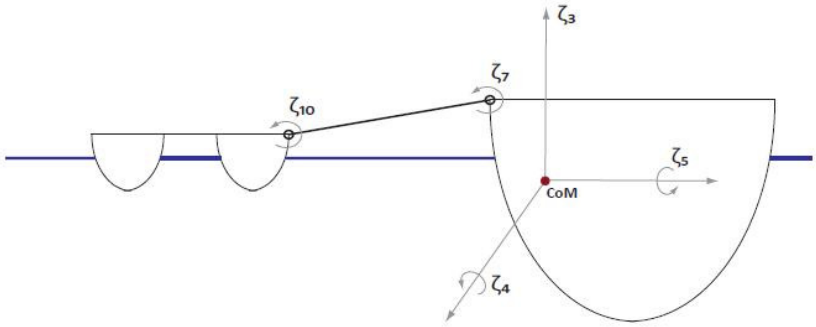

Figure 5.4.1: Constrained degrees of freedom for sea base

With expressions derived for the generalized coordinate system, potential energy, and kinetic energy the Lagrangian method is applied to the system to determine generalized accelerations for the coordinates considered.

$$\begin{aligned} F_{z_1} + F_{z_2} + F_{z_3} &= (m_1 + m_2 + m_3)g + (m_1 + m_2 + m_3)\ddot{\zeta}_3 \\ &+ \left(m_1 y_{c_1}^0 + m_2 y_{c_2}^0 + m_3 y_{c_3}^0\right)\ddot{\zeta}_4 - \left(m_1 x_{c_1}^0 + m_2 x_{c_2}^0 + m_3 x_{c_3}^0\right)\ddot{\zeta}_5 \\ &+ \left[m_1\left(y_{c_1}^0 - y_{p_1}\right)\right]\ddot{\zeta}_7 + \left[m_2\left(y_{c_2}^0 - y_{p_2}\right) + m_3\left(y_{c_2}^0 - y_{p_2}\right)\right]\ddot{\zeta}_{10} \end{aligned} \tag{5.29}$$

$$
\begin{aligned}
&M_{x_1}+M_{x_2}+M_{x_3}+F_{z_1}y_{c_1}^0+F_{z_2}y_{c_2}^0+F_{z_3}y_{c_3}^0-F_{y_1}z_{c_1}^0-F_{y_2}z_{c_2}^0-F_{y_3}z_{c_3}^0\\
&-\left(m_1gy_{c_1}^0+m_2gy_{c_2}^0+m_3gy_{c_3}^0\right)=\left(m_1y_{c_1}^0+m_2y_{c_2}^0+m_3y_{c_3}^0\right)\ddot{\zeta}_3\\
&+\left[m_1\left[\left(y_{c_1}^0\right)^2+\left(z_{c_1}^0\right)^2\right]+m_2\left[\left(y_{c_2}^0\right)^2+\left(z_{c_2}^0\right)^2\right]+m_3\left[\left(y_{c_3}^0\right)^2+\left(z_{c_3}^0\right)^2\right]+I_{x_1}+I_{x_2}+I_{x_3}\right]\ddot{\zeta}_4\\
&-\left(m_1y_{c_1}^0x_{c_1}^0+m_1y_{c_2}^0x_{c_2}^0+m_1y_{c_3}^0x_{c_3}^0\right)\ddot{\zeta}_5+\left[m_1\left[y_{c_1}^0\left(y_{c_1}^0-y_{p_1}\right)+z_{c_1}^0\left(z_{c_1}^0-z_{p_1}^0\right)\right]+I_{x_1}\right]\ddot{\zeta}_7\\
&+\left[m_2\left[y_{c_2}^0\left(y_{c_2}^0-y_{p_2}\right)+z_{c_2}^0\left(z_{c_2}^0-z_{p_2}^0\right)\right]\right.\\
&\left.+m_3\left[y_{c_3}^0\left(y_{c_3}^0-y_{p_3}\right)+z_{c_3}^0\left(z_{c_3}^0-z_{p_3}^0\right)\right]+I_{x_2}+I_{x_3}\right]\ddot{\zeta}_{10}
\end{aligned}
\tag{5.30}
$$

$$
\begin{aligned}
&M_{y_1}+M_{y_2}+M_{y_3}-F_{z_1}x_{c_1}^0-F_{z_2}x_{c_2}^0-F_{z_3}x_{c_3}^0+F_{x_1}z_{c_1}^0+F_{x_2}z_{c_2}^0+F_{x_3}z_{c_3}^0\\
&+\left(m_1gx_{c_1}^0+m_2gx_{c_2}^0+m_3gx_{c_3}^0\right)=-\left(m_1x_{c_1}^0+m_2x_{c_2}^0+m_3x_{c_3}^0\right)\ddot{\zeta}_3\\
&-\left(m_1x_{c_1}^0y_{c_1}^0+m_1x_{c_2}^0y_{c_2}^0+m_1x_{c_3}^0y_{c_3}^0\right)\ddot{\zeta}_4\\
&+\left[m_1\left[\left(x_{c_1}^0\right)^2+\left(z_{c_1}^0\right)^2\right]+m_2\left[\left(x_{c_2}^0\right)^2+\left(z_{c_2}^0\right)^2\right]\right.\\
&\left.+m_3\left[\left(x_{c_3}^0\right)^2+\left(z_{c_3}^0\right)^2\right]+I_{y_1}+I_{y_2}+I_{y_3}\right]\ddot{\zeta}_5-\left[m_1x_{c_1}^0\left(y_{c_1}^0-y_{p_1}\right)\right]\ddot{\zeta}_7\\
&-\left[m_2x_{c_2}^0\left(y_{c_2}^0-y_{p_2}\right)+m_3x_{c_3}^0\left(y_{c_3}^0-y_{p_3}\right)\right]\ddot{\zeta}_{10}
\end{aligned}
\tag{5.31}
$$

$$
\begin{aligned}
&M_{x_1}-F_{z_1}y_{p_1}^0-F_{y_1}z_{p_1}^0=m_1g\left(y_{c_1}^0-y_{p_1}\right)+\left[m_1\left(y_{c_1}^0-y_{p_1}\right)\right]\ddot{\zeta}_3\\
&+\left[m_1\left[y_{c_1}^0\left(y_{c_1}^0-y_{p_1}\right)+z_{c_1}^0\left(z_{c_1}^0-z_{p_1}\right)\right]+I_{x_1}\right]\ddot{\zeta}_4\\
&-\left(m_1x_{c_1}^0y_{c_1}^0+m_1x_{c_2}^0y_{c_2}^0+m_1x_{c_3}^0y_{c_3}^0\right)\ddot{\zeta}_4-\left[m_1x_{c_1}^0\left(y_{c_1}^0-y_{p_1}\right)\right]\ddot{\zeta}_5\\
&+\left[m_1\left[\left(y_{c_1}^0-y_{p_1}\right)^2+\left(z_{c_1}^0-z_{p_1}\right)^2\right]+I_{x_1}\right]\ddot{\zeta}_{10}
\end{aligned}
\tag{5.32}
$$

$$
\begin{aligned}
&M_{x_2}+M_{x_3}-F_{z_2}y_{p_2}-F_{z_3}y_{p_2}-F_{y_2}z_{p_2}+F_{y_3}z_{p_2}=m_2g\left(y_{c_2}^0-y_{p_2}\right)+m_3g\left(y_{c_3}^0-y_{p_2}\right)\\
&+\left[m_2\left(y_{c_2}^0-y_{p_2}\right)+m_3\left(y_{c_3}^0-y_{p_2}\right)\right]\ddot{\zeta}_3\\
&+\left[m_2\left[y_{c_2}^0\left(y_{c_2}^0-y_{p_2}\right)+z_{c_2}^0\left(z_{c_2}^0-z_{p_2}^0\right)\right]+I_{x_2}+I_{x_3}\right]\ddot{\zeta}_4\\
&-\left[m_2x_{c_2}^0\left(y_{c_2}^0-y_{p_2}\right)+m_3x_{c_3}^0\left(y_{c_3}^0-y_{p_2}\right)\right]\ddot{\zeta}_5\\
&-\left[m_2\left[\left(y_{c_2}^0-y_{p_2}\right)^2+\left(z_{c_2}^0-z_{p_2}\right)^2\right]+m_3\left[\left(y_{c_3}^0-y_{p_2}\right)^2+\left(z_{c_3}^0-z_{p_2}\right)^2\right]+I_{x_2}+I_{x_3}\right]\ddot{\zeta}_{10}
\end{aligned}
\tag{5.33}
$$

These equations form the basis for calculating the motion of the 3-body system. The hydrodynamic forces are received from AEGIR while additional forces are added from the air cushion as well as various control methods. The linearized form of the Lagrangian allowed for simple calculations when solving for the accelerations. The classical 4th order Runga-Kutta method is then used to determine the new position at each time step and the process is repeated. Further explanation into the air cushion model employed as well as the control forcing is provided in further detail in proceeding sections.

5.5 Wave Modeling

In the SimMechanics model, a single sine wave with noise was used to roughly mimic filtered noise in an attempt to match a wave profile with only one input. AEGIR allows a user defined number of sine waves removing the limitations placed on the previous model. As such, a more comprehensive method for determining the sine waves comprising the wave front is presented.

Once again, though stochastic in nature, wave fronts can be approximated by a superposition of sine waves.

$$\zeta(x,t) = \sum_{i=1}^{N} A_i \sin(\omega_i t - k_i x + \phi_i) \tag{5.34}$$

There are a number of models used to approximate wave spectrums. By using an appropriately selected model for the spectrum, the constants for the sine waves are

solved and implemented in AEGIR. The two widely used models are the Pierson Moskowitz spectrum and the JONSWAP spectrum. The Pierson Moskowitz spectrum is used for fully developed wave conditions while the JONSWAP spectrum is used for developing wave conditions with the idea that no wave front is ever fully developed. Waves continue to develop through non-linear wave-wave interactions over long periods of time. The Pierson Moskowitz spectrum assumes that at some point the waves and wind reach an equilibrium point where the waves no longer grow.

For this system, the Pierson Moskowitz spectrum was used because it allows for a maximum limit to be placed on the type of waves encountered by the vessels. While they would be exposed to growing waves in other operations, during cargo transfer the maximum amount of waves present would be from a sea state 4 classification. As a result, it is not necessary to allow waves to develop past this point as the procedure would not be carried out after exceeding that classification. The Pierson Moskowitz spectrum for fully developed sea states, roughly 10,000 wave cycles, in deep sea water [14] is

$$S(\omega) = \frac{\alpha g^2}{\omega^5} \exp\left[-\beta \left(\frac{\omega_0}{\omega} \right)^4 \right] \tag{5.35}$$

where g is gravity, ω is the angular frequency, ω_0 is $\frac{g}{U_{19.5}}$ with $U_{19.5}$ being the wind speed 19.5 meters above sea level, α is 8.1×10^{-3}, and β is function of the wind speed generating the waves. The peak frequency is the dominant frequency over a range of

frequencies comprising the wave front. The peak frequency can be easily determined by setting the derivative of the spectrum with respect to the frequencies equal to zero. Due to the nature of the spectrum shape, this results in the positive extremum of the curve.

$$\frac{d}{d\omega}S(\omega_p) = -5\frac{\alpha g^2}{\omega^6}\exp\left[-\beta\left(\frac{\omega_0}{\omega}\right)^4\right] - 4\beta\left(\frac{\omega_0^4}{\omega^5}\right)\frac{\alpha g^2}{\omega^5}\exp\left[-\beta\left(\frac{\omega_0}{\omega}\right)^4\right]$$

$$0 = -5\frac{\alpha g^2}{\omega_p^6}e^{-\beta f(\omega)} + 4\beta\frac{\alpha g^2\omega_0^4}{\omega_p^{10}}e^{-\beta f(\omega)}$$

$$\omega_p^4 = \frac{4\beta}{5}\omega_0^4$$

$$\omega_p = \omega_0\left(\frac{4\beta}{5}\right)^{1/4} \tag{5.36}$$

With this formulation the value of ω_0 is solved from the peak angular frequency specified by the profile used. Finally, the wind dependent value of β can be calculated from its dependence on significant wave height, H_s. Typically, the wind speed determines the wave height (and therefore β) but because the problem specifies the wave characteristics, it allows for the value to be solved directly

$$\beta = \frac{3.11}{H_s^2\omega_0^4} \tag{5.37}$$

The following table gives observed relevant values for various sea states

Table 5.5.1: Sea state table values [15]

Wind Speed	Sea State	Wave Height (m)	Average Period (s)	Average Wave Length (m)
14	3	1.0668	3.5	14.0208
15	3	1.2192	4	16.002
16	3.5	1.3716	4	17.9832
17	3.5	1.524	4.5	19.9644
18	4	1.8288	5	24.0792
19	4	2.1336	5	28.0416
20	4	2.286	5.5	30.1752

Using the table and formulas it becomes simple to recreate the spectrum for a given sea state. Figure 5.3.1 shows three sea states created for dominant modal periods of 4,5, and 6 seconds.

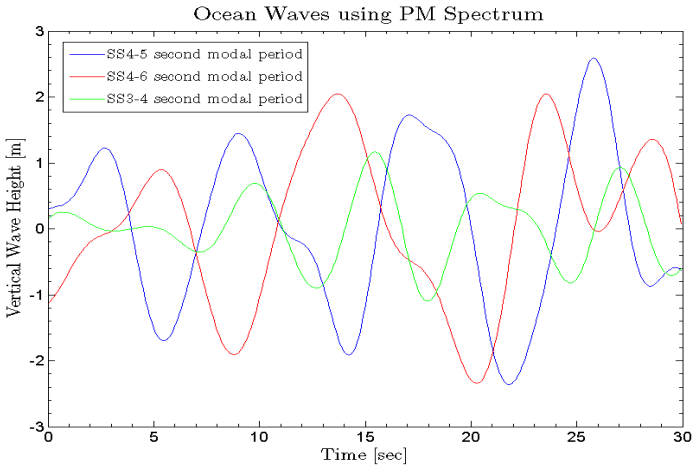

Figure 5.5.1: Wave outputs for various sea conditions

The last step involves breaking down the spectrum into a series of sine waves. This is done by relating the area under a portion of the power spectrum to an amplitude related to the frequency at that portion of the spectrum. Namely, the area under the spectrum is equal to half of the sum of amplitudes squared

$$\int_0^{\omega_{\max}} S(\omega)\, d\omega = \frac{1}{2}\sum_i^n A_i^2 \qquad for \qquad i = 1, 2, ..., n \tag{5.38}$$

Now breaking the spectrum down into 100 components and representing the area between each frequency with a single sine wave and using the rectangular method to solve for integral area gives

$$S(\omega_0 + \Delta\omega \times i)\,\Delta\omega = \frac{1}{2} A_i^2 \quad for \;\; i = 1, 2, ..., 100 \tag{5.39}$$

Adding a random phase between 0 and 2π completes the requirements for the wave decomposition into sine waves. The corresponding values are added to a table and imported into AEGIR through a text file. The wave output and further wave-wave interactions are all handled internally within AEGIR.

5.6 Free Surface Modeling

The free surface of a fluid is the boundary where the fluid undergoes constant perpendicular stress with zero shear stress. An example of this occurrence is at the contact between two fluids such as water and air. Disturbances along free surfaces results in waves such as ocean waves generated from wind resistance. In AEGIR, user input is required to define the topology of the free surfaces in order to formulate their deformations. Additionally, AEGIR solves for the deformations along the free surfaces differently depending on its interface with the vessels present within them. The first of three main types of free surface interfaces is the transom free surface

(TFS) patch that occurs when a vessel has a flat stern making contact at sea level. If the vessel is contoured at each end then formulation is simpler and fewer instabilities arise when simulating these vessels. The other main types of free surfaces are inner free surfaces (IFS) and outer free surfaces (OFS). The inner free surface is the patch of water between vessels for multi body simulations that extends to the edge of the ocean domain. The outer free surface is simply the two patches on the outer most region of domain beyond the edge of the outside vessel(s) and the open ocean. Figure 5.6.1 shows a top view illustration of the ships and examples of each type of patch.

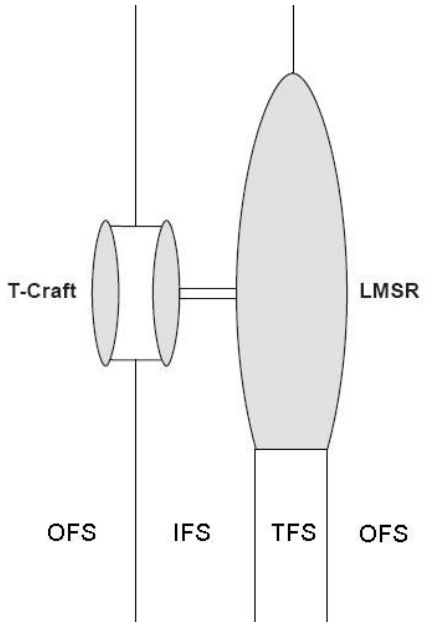

Figure 5.6.1: Top view of sea base and free surface descriptions

Typically no special attention is required in contracting free surface patches in AEGIR as the program includes templates for simple multi body configurations. However, this particular configuration is unusual and no such template exists. AEGIR normally handles each body individually and attempts to construct free surface patches

between every vessel in the simulation domain. Since the T-Craft is actually a single vessel constructed using two bodies with an unusual contact region with the water, the free surface patches were constructed manually and imported into AEGIR. This meant eliminating the inner free surface between the catamaran hulls and extending the outer and inner free surfaces to the midpoint of the bow and stern. When manually constructing free surfaces, the aspect ratio of each patch must be approximately the same order. As a result, testing needed to be done to establish proper meshing and spacing of the patches to ensure simulation stability. Figure 5.6.2 shows the completed free surface patches created in Rhino.

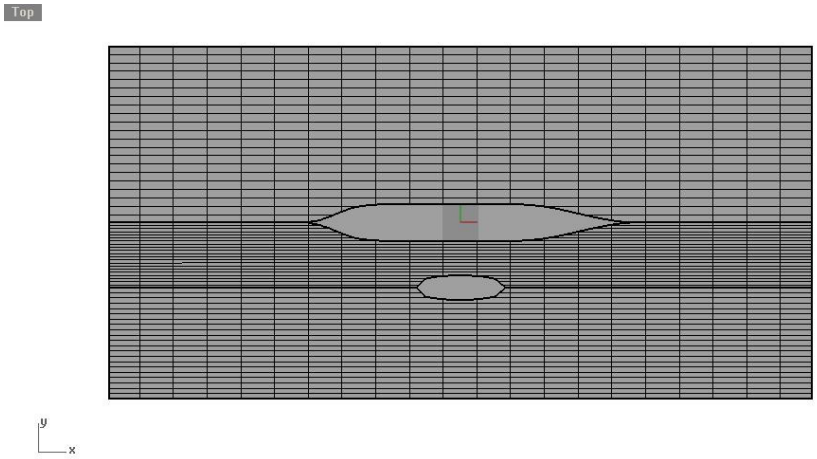

Figure 5.6.2: Top view of free surface patch created in Rhino3d

In order to import this free surface profile into AEGIR, a third program provided by Navatek was used to format the RHINO file into a compatible input into AEGIR. Once imported, the rest of the properties are input as text files normally used by AEGIR.

5.7 Interfacing

While AEGIR can act as a standalone program capable of incorporating some simple internal forcing, the features for incorporating sophisticated forcing algorithms are limited. As a result, in order to implement control into the system, AEGIR is used modularly solely for its hydrodynamic component. In order to accomplish this, a TCP/IP connection is established with AEGIR using code implemented in Matlab.

Due to limitations in the software, interfacing Aegir with other programs eliminates the motion solver component of the program. As such, this portion is incorporated in the Matlab code itself. Lagrangian Mechanics are used to derive the subsequent equations as previously explained. Figure 5.7.1 gives a clear portrait of how the system is simulated at each time step.

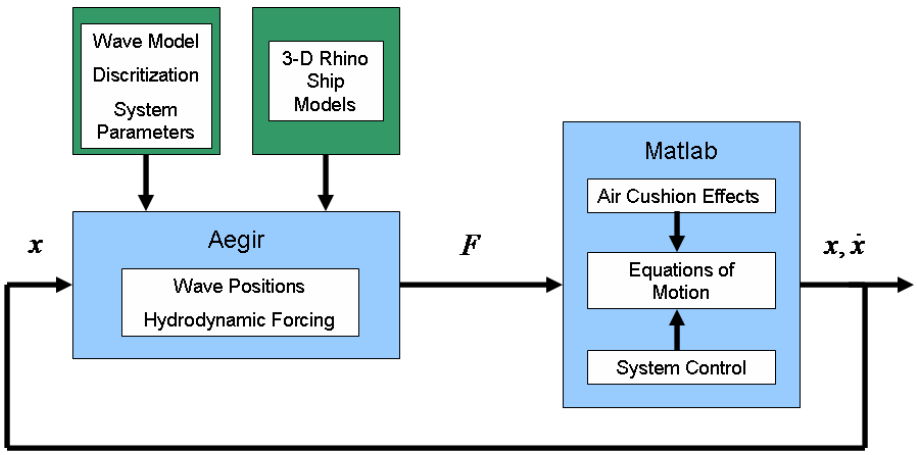

Figure 5.7.1: Aegir environment interfacing information flow chart

AEGIR uses a set of static parameters that determine the characteristics of the system. This includes things like domain size, discretization, hull definitions, etc.

These parameters are introduced through text files and incorporated initially by AEGIR. AEGIR then incorporates the CAD models and checks the geometry for inconsistencies. Once complete, the hulls and free surfaces are meshed and the analysis begins. At the first time step, AEGIR sends positional data as well as the wave forcing including added mass. These forces are integrated with the forces from the air cushion as well as forces provided by the controller. Once combined, the equations of motion are solved for a single time step determining the new position of the system. This information is then sent back to AEGIR. The process is repeated with subsequent positioning information from AEGIR discarded in favor of the calculated ones.

This process allows much more freedom in choosing controllers. Previously, control forces were either limited in implementation or required specific modeling technique to integrate. However, with this method the user has total freedom to create and implement a controller as desired.

Chapter 6 AEGIR Model Control Law

The previous sections explained the details of the system setup. With the system established, two methods were developed to control the system. The first method relies on passive control to damp the motion between the ramp itself and the vessels. The second method is an active controller that seeks to use the dynamics of the T-Craft to reduce the motion of the ramp.

6.1 Active control using Backstepping

In this section a controller is developed using backstepping to control the air flow into the air cushion. By controlling the air flow, the pressure can be appropriately altered to maintain a desirable heave. Due to the size disparity and design differences between the vessels, the T-Craft experiences much larger displacements than the LMSR. As a result, reducing the heave of the T-Craft reduces the relative heave between the vessels and thus the ramp oscillations themselves. Additionally, there is no way to control the movement of the LMSR internally. As a result, all of the control effort is placed on the T-Craft.

The method employed to develop a control law was backstepping. Backstepping is a control method that is optimally employed on a system containing controllable subsystems. The states of the system at its "base" are used as virtual controllers. As the user backs out of the stable subsystem to new outer layers, new virtual controllers are designed that guarantees stability of each new outer layer while

maintaining the control of the original subsystems. The process uses Lyapunov functions to determine control laws at each step and error terms replace the original states to denote the difference between the desired value and actual value. This transformation takes the following system [16]

$$\begin{aligned} \dot{x}_1 &= f_1(x_1, x_2) \\ \dot{x}_2 &= x_3 + f_2(x_1, x_2) \\ \dot{x}_3 &= u + f_3(x_1, x_2, x_3) \end{aligned} \tag{6.1}$$

and transforms it into the following system

$$\begin{aligned} \dot{x}_1 &= f_x(x) + g_x(x) z_1 \\ \dot{z}_1 &= f_1(x, z_1) + g_1(x, z_1) z_2 \\ \dot{z}_2 &= f_2(x, z_1, z_2) + g_2(x, z_1, z_2) u \end{aligned} \tag{6.2}$$

where z_i are state error terms, g_i are virtual controllers, and u is the final control law. To begin, the system needs to be written in state space form. Control laws are then determined for each subsystem in terms of a Lyapunov function that guarantees stability. The system is then expressed in terms of the virtual controller error and the process repeated until the input is reached and a final control law is determined.

In order to use this design method, the dynamics of the T-Craft must to be integrated into the dynamics of the air cushion and the input into the system. Taking the full dynamics of the equations of motion would produce a system containing difficult terms with regards to employing this method. Instead, a decoupled approach is used from literature that relates the degrees of freedom of a craft a spring mass damper equation with sinusoidal inputs. This approximation was used earlier to create a rigid body formulation of the system. Here, it serves as a method to introduce heave

motion deterministically (although approximately) without needing to account for other states that are of little interest. Once again, the equation used for heave of the system is

$$\left(m+m_A\right)\ddot{x}_h+b\dot{x}_h+kx_h=F \tag{6.3}$$

where m is craft mass, m_A is added mass, b and k are damping and stiffness terms respectively, and F is the forcing. The constants are determined beforehand as in the first section, given through design criteria, or provided by AEGIR at each time step. Note that in the previous simulations, the added mass term was treated as a constant due to limitations in calculating this term. Aegir solves this term and returns it to the user in a state vector, therefore this value is time dependant but also readily available. For simplicity, the mass and added mass are lumped into one mass term for derivation, however the proper updating value is used within the simulation. For the air cushion and ship dynamics, the pressure formulation and heave equation of motion was rewritten using the following states.

$$\begin{aligned} x_1 &= h \\ x_2 &= \dot{x}_1 \\ x_3 &= P \\ u &= q_{in} \end{aligned} \tag{6.4}$$

where h is heave, P is air cushion pressure, and q_{in} is the air flow into the air cushion. Using these states in the formulation for heave and air cushion dynamics yields the following state space representation

$$\begin{aligned}\dot{x}_1 &= x_2 \\ \dot{x}_2 &= -\frac{C_{33}}{m}x_1 - \frac{B_{33}}{m}x_2 + \frac{A_0}{m}x_3 \\ \dot{x}_3 &= \frac{-\gamma P_0}{h_0}x_2 - \frac{1}{C_c R_L}x_3 + \frac{1}{C_c}u\end{aligned} \tag{6.5}$$

Now the goal is to stabilize x_1 and x_2 using x_3 as a virtual controller, ξ. Rewriting the subsystem substituting x_3 with the virtual controller yields

$$\begin{aligned}\dot{x}_1 &= x_2 \\ \dot{x}_2 &= -\frac{C_{33}}{m}x_1 - \frac{B_{33}}{m}x_2 + \frac{A_0}{m}\xi\end{aligned}$$

For this, a relatively straightforward Lyapunov function is chosen with the coefficients selected to eliminate some of the terms in the derivative

$$V(x) = \frac{C_{33}}{2m}x_1^2 + \frac{1}{2}x_2^2 \tag{6.6}$$

Using Khalil's theorem 4.1 [17], for $V(0)=0$ and $V(x)>0$ over the domain containing the equilibrium point $x=0$, if $\dot{V}(x)\le 0$ over the same domain then $x=0$

is stable. To determine the virtual controller to satisfy these conditions, the derivative of the Lyapunov function is determined and set to be less than or equal to zero.

$$\dot{V}(x_1, x_2) = \frac{\partial V}{\partial x_1}(x)\dot{x}_1 + \frac{\partial V}{\partial x_2}(x)\dot{x}_2$$
$$= \left(\frac{C_{33}}{m}x_1\right)\dot{x}_1 + x_2\dot{x}_2 = \left(\frac{C_{33}}{m}x_1\right)x_2 + \left(-\frac{C_{33}}{m}x_1 - \frac{B_{33}}{m}x_2 + \frac{A_0}{m}\xi\right)x_2$$
$$\dot{V}(x_1, x_2) = -\frac{B_{33}}{m}x_2^2 + \frac{A_0}{m}\xi x_2 \leq 0 \tag{6.7}$$

The term $-\frac{B_{33}}{m}x_2^2$ is already less than or equal to zero as both B_{33} and $m > 0$. Similarly, since $A_0 \succ 0$ by letting the virtual controller be

$$\xi = -c_1 x_2 \tag{6.8}$$

the second term is also less than or equal to zero. This turns the derivative of the Lyapunov into

$$\dot{V}(x_1, x_2) = -\frac{B_{33}}{m}x_2^2 - c_1\frac{A_0}{m}x_2^2$$
$$\dot{V}(x_1, x_2) = -\frac{1}{m}(B_{33} + c_1 A_0)x_2^2 \tag{6.9}$$

Here $\dot{V}(x) = 0$ over the line of $x_2 = 0$. However, using the virtual control input we see from $\dot{x}_2 = -\frac{C_{33}}{m}x_1 - \left(\frac{B_{33}}{m} - \frac{c_1 A_0}{m}\right)x_2$ that on the line $x_2 = 0$ that the only

solution that satisfies $\dot{V}(x)=0$ is when $x_1=0$. By Lasalles's Theorem $[17]$, the system meets stability criterion and the heave converges to a constant value. However, this is only the first step as ξ is only the virtual controller and does not use the real control input. To do so the system is augmented using the virtual controller and an error term. The error term is defined as

$$z=\xi-\xi_{des} \tag{6.10}$$

and letting the desired value of the virtual controller be the value to stabilize the original subsystem, $\xi_{des}=-c_1x_2$, and also computing its derivative gives

$$\begin{aligned} z&=\xi+c_1x_2\\ \dot{z}&=\dot{\xi}+c_1\dot{x}_2 \end{aligned} \tag{6.11}$$

This is now used to rewrite the system in terms of this error variable which gives

$$\begin{aligned} \dot{x}_1&=x_2\\ \dot{x}_2&=-\frac{C_{33}}{m}x_1-\frac{B_{33}}{m}x_2+\frac{A_0}{m}(z-c_1x_2)\\ \dot{z}_3&=\frac{-\gamma P_0}{h_0}x_2-\frac{1}{C_cR_L}(z-c_1x_2)+\frac{1}{C_c}u+c_1\left[-\frac{C_{33}}{m}x_1-\frac{B_{33}}{m}x_2+\frac{A_0}{m}(z-c_1x_2)\right]\\ &=-\frac{c_1C_{33}}{m}x_1+\left(\frac{-\gamma P_0}{h_0}+\frac{c_1}{C_cR_L}-\frac{c_1B_{33}}{m}-\frac{c_1^2}{m}\right)x_2+\left(-\frac{1}{C_cR_L}+\frac{c_1A_0}{m}\right)z+\frac{1}{C_c}u \end{aligned} \tag{6.12}$$

Once again a Lyapunov function is selected to create a control law for the system. The function is chosen as the original function with an added quadratic term for the error of the virtual controller with its derivative being

$$V_z(x_1, x_2, z) = \frac{C_{33}}{2m} x_1^2 + \frac{1}{2} x_2^2 + \frac{1}{2} z^2 \tag{6.13}$$

$$\begin{aligned}\dot{V}_z(x_1, x_2, z) &= \frac{\partial V}{\partial x_1}(x)\dot{x}_1 + \frac{\partial V}{\partial x_2}(x)\dot{x}_2 + \frac{\partial V}{\partial z}(z)\dot{z} = \frac{C_{33}}{m} x_1\dot{x}_1 + x_2\dot{x}_2 + z\dot{z} \\ &= \frac{C_{33}}{2m} x_1 x_2 + \left[-\frac{C_{33}}{m} x_1 - \frac{B_{33}}{m} x_2 + \frac{A_0}{m}(z - c_1 x_2) \right] x_2 + \\ &+ \left[-\frac{c_1 C_{33}}{m} x_1 + \left(\frac{-\gamma P_0}{h_0} + \frac{c_1}{C_c R_L} - \frac{c_1 B_{33}}{m} - \frac{c_1^2}{m} \right) x_2 + \left(-\frac{1}{C_c R_L} + \frac{c_1 A_0}{m} \right) z + \frac{1}{C_c} u \right] z\end{aligned}$$

$$\begin{aligned}\dot{V}_z(x_1, x_2, z) = &-\frac{c_1 C_{33}}{m} x_1 z + \left(-\frac{B_{33}}{m} - \frac{c_1 A_0}{m} \right) x_2^2 + \left(-\frac{\gamma P_0}{h_0} + \frac{c_1}{C_c R_L} - \frac{B_{33}}{m} - \frac{c_1^2 A_0}{m} + \frac{A_0}{m} \right) x_2 z \\ &+ \left(-\frac{1}{C_c R_L} + \frac{c_1 A_0}{m} \right) z^2 + \frac{1}{C_c} uz\end{aligned} \tag{6.14}$$

Realizing that the terms $\left(-\frac{B_{33}}{m} - \frac{c_1 A_0}{m} \right) x_2^2$ are negative definite under any circumstances, choosing a controller to set the rest of the Lyapunov derivative equal to the negative definite $-c_2 z^2$ in order to satisfy the necessary conditions for stability yields

$$\begin{aligned}-c_2 z^2 = &-\frac{c_1 C_{33}}{m} x_1 z + \left(-\frac{B_{33}}{m} - \frac{c_1 A_0}{m} \right) x_2^2 + \left(-\frac{\gamma P_0}{h_0} + \frac{c_1}{C_c R_L} - \frac{B_{33}}{m} - \frac{c_1^2 A_0}{m} + \frac{A_0}{m} \right) x_2 z \\ &+ \left(-\frac{1}{C_c R_L} + \frac{c_1 A_0}{m} \right) z^2 + \frac{1}{C_c} uz\end{aligned}$$

then solving for u

$$u = -C_c\left[\frac{c_1 C_{33}}{m}x_1 + \left(-\frac{\gamma P_0}{h_0} + \frac{c_1}{C_c R_L} - \frac{B_{33}}{m} - \frac{c_1^2 A_0}{m} + \frac{A_0}{m}\right)x_2 + \left(-\frac{1}{C_c R_L} + \frac{c_1 A_0}{m}\right)z\right] - C_c c_2 z \quad (6.15)$$

with $c_2 \succ 0$. This reduces the Lyapunov function derivative to

$$\dot{V}_z(x_1, x_2, z) = -\left(\frac{B_{33}}{m} + \frac{c_1 A_0}{m}\right)x_2^2 - c_2 z^2 \quad (6.16)$$

Once again using LaSalle's theorem, we can see that the heave converges to a steady value and the system is stable. Finally, replacing the virtual controller error term with the original state values gives the final controller as

$$u = -C_c\left[\frac{c_1 C_{33}}{m}x_1 + \left(-\frac{\gamma P_0}{h_0} + \frac{c_1}{C_c R_L} - \frac{B_{33}}{m} - \frac{c_1^2 A_0}{m} + \frac{A_0}{m}\right)x_2 + \left(-\frac{1}{C_c R_L} + \frac{c_1 A_0}{m}\right)(x_3 + c_1 x_2)\right]$$
$$-C_c c_2 (x_3 + c_1 x_2)$$
$$u = \left(\frac{c_1 C_{33} C_c}{m}\right)x_1 - C_c\left(-\frac{\gamma P_0}{h_0} - \frac{B_{33}}{m} + \frac{A_0}{m} + c_1 c_2\right)x_2 - C_c\left(-\frac{1}{C_c R_L} + \frac{c_1 A_0}{m} + c_2\right)x_3 \quad (6.17)$$

To summarize, this controller was developed using the uncoupled equation for heave along with the air cushion pressure dynamics. The final controller is used to regulate the air flow into the air cushion that will then affect the lift due to the change in pressure. All of the necessary variables are tracked by AEGIR and the control law gives a pressure term that is incorporated into the equations of motion as a forcing term using the derivation for air cushion lift determined earlier.

6.2 Passive Control

This method of control attempts to reduce the ramp oscillation by applying a restoring force to each vessel when the displacement of the ramp is outside the equilibrium range. Much like a suspension in an automobile is tuned to restore position to a desired height, a tensional spring damper is considered to restore ramp angles to a desired initial state. Using Hooke's Law for an angular spring gives

$$\tau_s = -\kappa_s \theta \tag{6.18}$$

where τ_s is the applied moment, θ is the ramp angle deviation from equilibrium, and κ_s is the spring constant within the elastic range of the spring.

Similarly, a damper is jointly considered to further reduce the oscillation with the torsion spring. The form for a torsion damper follows the same form as a linear damper except it responds to angular velocity

$$\tau_d = -\kappa_d \dot{\theta} \tag{6.19}$$

where τ_d is the applied moment, $\dot{\theta}$ is the angular velocity of the ramp, and κ_d is the spring constant within the elastic range of the spring. The spring dampers are placed at each corner of the ramp between the vessels and the underside of the ramp.

Typically, the selection of the values for each the spring and damper requires careful analysis. However, in this instance the limiting factor is the strength of the components relative to the required optimal moments of the system. Due to the size of the vehicles and the disturbances they meet, the most powerful torsion dampers available will not negatively impact the vessels by over damping the system. Also, unlike the automobile example where an excessively powerful spring would negate the effectiveness of the controller, in this system an excessively stiff spring would not only make controller ineffective but also unstable.

As a result, the most powerful springs and dampers available were tested for effectiveness. Table 5.2.1 gives the stiffness and damping values, manufacturers and weight of each component.

Table 5.2.1: Spring and damper values

Component	**Manufacturer**	**Weight**	**Stiffness/Damping Value**
Spring	MW Industries	150 Kg	10^9 Nm/rad
Damper	Efdyn	25 Kg	10^3 Nm/rad/s

While the torque available is not enough to destabilize the system, the issue of design feasibility would need to be addressed by naval architects. During simulation, it is assumed that the interfaces between the spring dampers and their contact points are sufficiently strong to withstand the effect of the induced torque. Further investigation would be required if smaller values were to be used.

To add these torques to the simulation, after each time step the relative roll and roll velocity between each ship and the ramp is calculated. The appropriate moment is determined through the spring and damper constants and the resulting moment is added into the equations of motion as an internal force. The process is repeated at each time step for the duration of the simulation.

Chapter 7 Aegir Model Results

7.1 Active Control Results

In this section results for the active air cushion controller are presented. The system results for wave heading angles of 0° and 45° are presented. Any number of waves angles can be studied, these two were shown to show the effects of purely bow approaching waves as well as waves approaching from the lee side (T-Craft downwind from approaching waves) of the sea base. Some comparisons are also presented for the air cushion model with constant air flow.

Figure 6.1.1 shows the heave plot for the simple air cushion vehicle (ACV) mode in 0° and 45° wave heading angles. In this mode of operation the flow rate into the air cushion is constant. Figure 6.1.2 similarly shows the pitch angle of the T-Craft for headings of 0° and 45°. Finally, Figure 6.1.3 shows the roll angle of the T-Craft for headings of 0° and 45°. Wave heading is abbreviated to WH and sea state is abbreviated to SS in the figures.

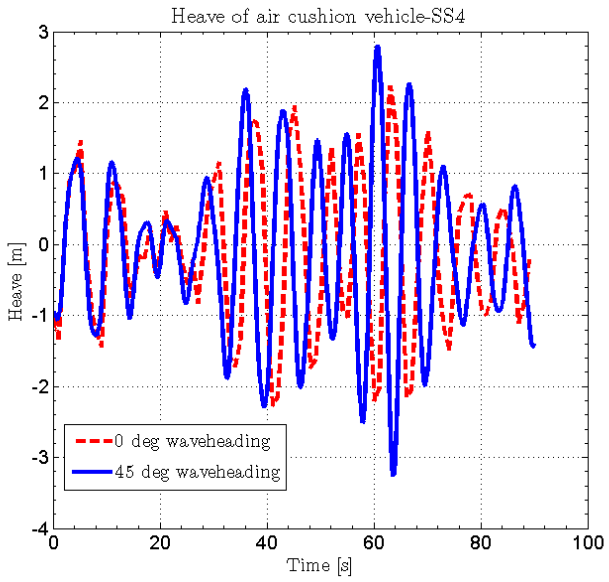

Figure 7.1.1: Heave of T-Craft in ACV mode -SS4 WH 0, 45 Deg

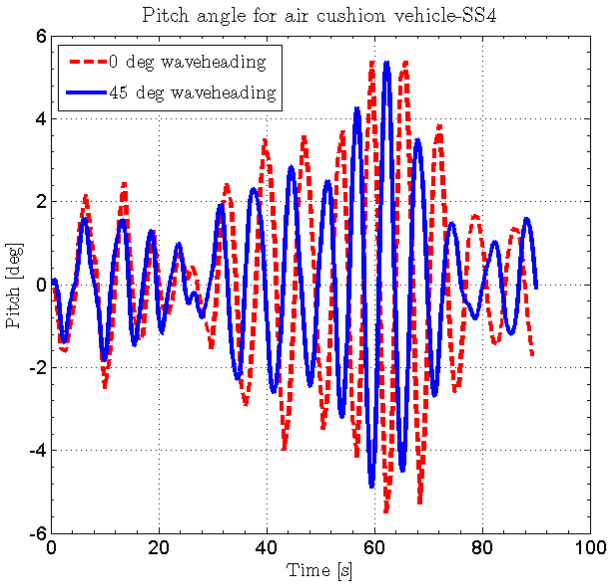

Figure 7.1.2: Pitch of T-Craft in ACV mode -SS4 WH 0, 45 Deg

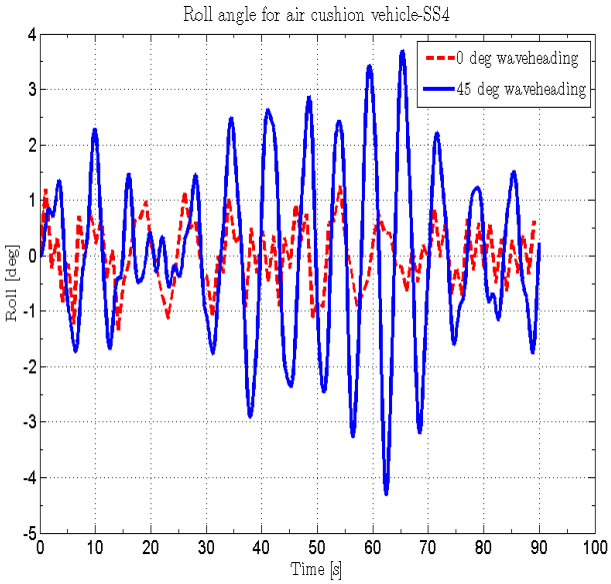

Figure 7.1.3: Roll of T-Craft in ACV mode -SS4 WH 0, 45 Deg

From the first two of those figures it is clear that there is not a significant difference in heave or pitch of the T-Craft when changing the wave heading angle. There is however a noticeable increase in T-Craft roll when operating in a wave heading of 45°. This result is intuitive as when heading directly into the waves the only contributing factor in roll is the ramp pivot forcing. This force is very small compared to the roll moment experienced by the T-Craft when waves are approaching from an angled front. It is important to note the controller was designed to maintain a steady heave in the T-Craft and not affect the other degrees of freedom. As such, the control will have less effect in environments where the roll contributes more significantly to the ramp pitch angle.

Figure 7.1.4 shows the heave of the T-Craft with and without control in a wave heading of 0°. Figure 7.1.5 shows the heave of the T-Craft with and without control in a wave heading of 45 degrees.

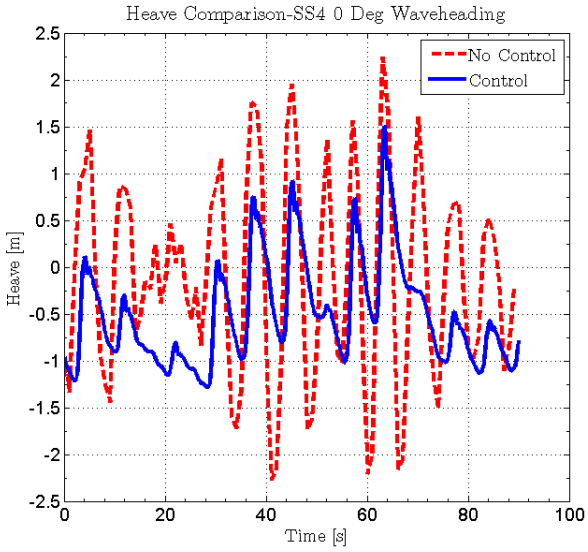

Figure 7.1.4: Heave Comparison of T-Craft with and without control -SS4 WH 0 Deg

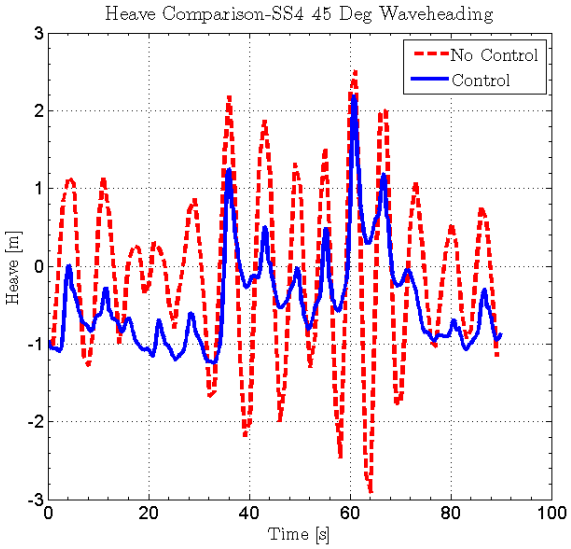

Figure 7.1.5: Heave Comparison of T-Craft with and without control -SS4 WH 45 Deg

The figures illustrate a significant reduction in T-Craft heave during the active air cushion controlled simulation. During the uncontrolled case, the T-Craft oscillates roughly 2-4 meters. When controlled, the air cushion is very good at rejecting the negative portion of the oscillation by filling up with air during this section. By doing this, the range of heave for the controlled case gets reduced by 1-1.5 meters. Additionally, by attempting to maintain the heave at a set height, the magnitude of oscillations gets subsequently reduced as well.

Figure 7.1.6 shows the pitch angle of the ramp with and without control for a wave heading of 0°. Figure 7.1.7 shows the pitch angle of the ramp with and without control for a wave heading of 45°.

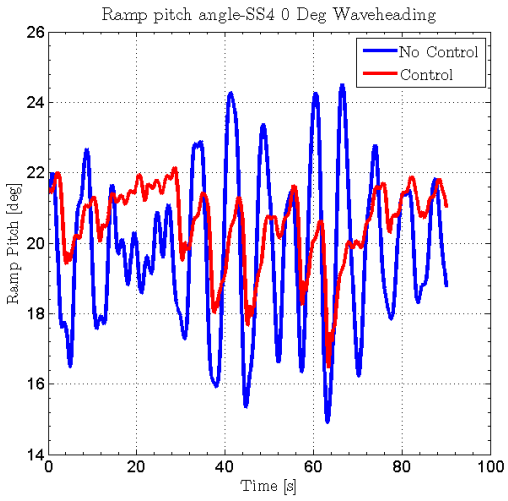

Figure 7.1.6: Ramp pitch angle with and without control -SS4 WH 0 Deg

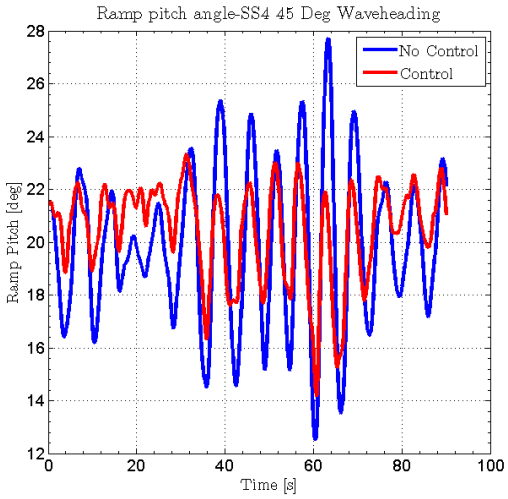

Figure 7.1.7: Ramp pitch angle with and without control -SS4 WH 45 Deg

As theorized, the controller is less effective in a wave heading of 45°. Never the less, the controller is effective in each case at reducing the maximum ramp deflection and also the magnitude of the overall deflection. This is clearly seen in Figure 7.1.8, where the standard deviation from the deflection mean is observed.

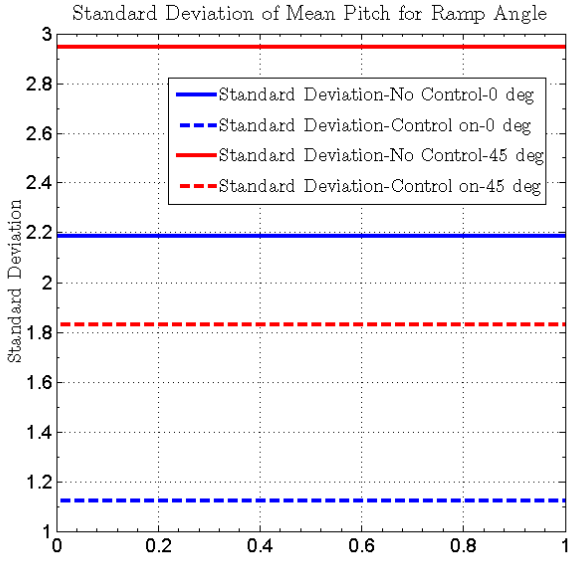

Figure 7.1.8: Standard deviation of ramp pitch angle -SS4 WH 0,45 Deg

In general the standard deviation is higher for the wave heading of 45° due to the added roll effect causing bouncing in the ramp pitch angle. While this behavior is bad, the current system setup does not allow for optimization over wave heading due to the static free surface approach that Aegir uses. Never the less, the controller is still effective and reducing some of the ramp oscillation due to heaving T-Craft. From Figure 7.1.8, a decrease in standard deviation of 1.1 is noticed in the both wave headings. The controllers is not only effective in reducing the overall pitch angle, but also the range of pitch angles experienced by the ramp during simulation.

To get an idea of the added forcing required by the T-Craft, Figure 7.1.9 illustrates the added necessary pressure created by the air cushion to reduce the heave.

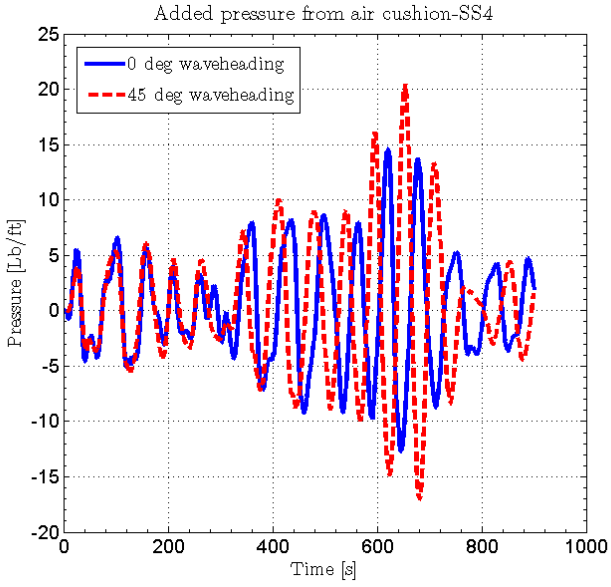

Figure 7.1.9: Required pressure change during control process -SS4 WH 0,45 Deg

It is important to note that the controller cannot create a negative air pressure in the controller. This figure instead shows the difference in pressure between controlled and uncontrolled simulations. Decrease in pressure arises from the air flow being set to zero and reduction of air pressure due to the linear escape term. This illustrates a potential problem with this type of controller. Instead of matching flow rate to capture a desired increase in pressure, the flow rate should be considered constant and the controller could capture a desired escape of air flow through a louver system.

7.2 Passive Control Results

This section outlines the effects of adding a spring and damper on the ramp at the ramp pivot points. The system was simulated in sea state 4 in wave heading angles of 0° and 45°. This is done to study the effect of directly approaching waves vs. an angled wave front approach. Figure 7.2.1 shows the ramp pitch angle for controlled and uncontrolled case in a wave heading angle of 0°. Figure 7.2.1 shows the ramp pitch angle for controlled and uncontrolled case in a wave heading angle of 45°.

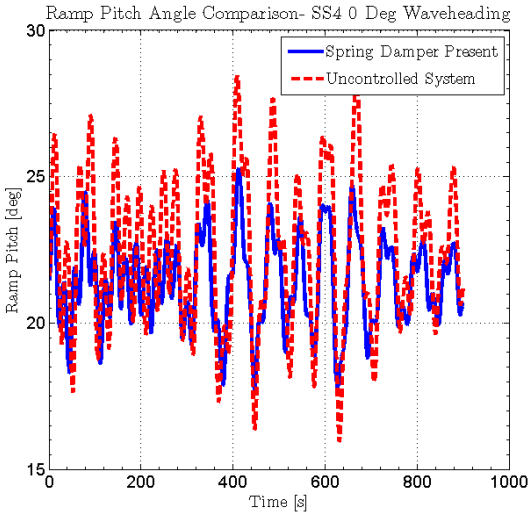

Figure 7.2.1: Ramp pitch angle Comparison -SS4 WH 0 Deg

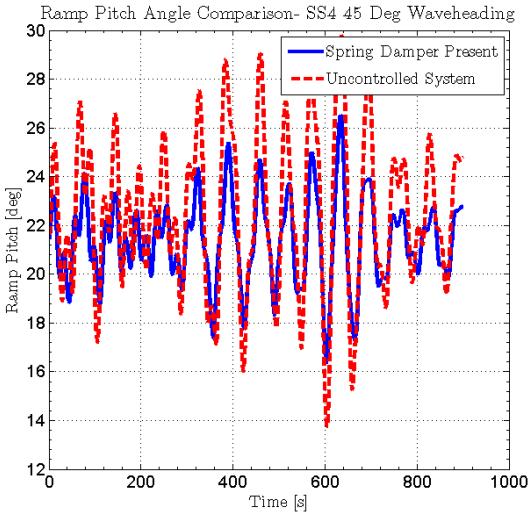

Figure 7.2.2: Ramp pitch angle Comparison -SS4 WH 45 Deg

In each case a reduction of ramp oscillation was observed. For the wave heading of 0°, the oscillation gets reduced from $\pm 7^{\circ}$ around the mean of 22.38° to $\pm 5^{\circ}$ around a mean of 21.33°. This reduces the standard deviation of ramp pitch angle from 2.6 down to 1.5. Similarly in a wave heading of 45°, the oscillation gets reduced

from $\pm 7^{\circ}$ around the mean of 22.40° to $\pm 5^{\circ}$ around a mean of 21.32°. The reduces the standard deviation of ramp pitch angle from 3.2 down to 1.8. The figures also illustrate that while also reducing the max deflection in ramp pitch angle, the controller also serves to minimize the overall oscillation amplitude. This is a desirable property as the final pitch angle is of little consequence compared to the magnitude of its oscillations. The controller is slightly less effective in the 45° wave heading angle. This can be partially explained by Figures 7.2.3 and 7.2.4. Each shows the T-Craft roll for the controlled and uncontrolled cases for each wave heading angle.

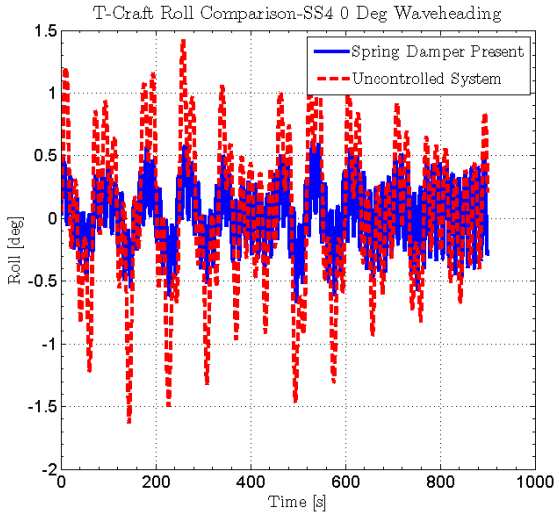

Figure 7.2.3: Roll comparison for controlled vs. uncontrolled system- SS4 WH 0 Deg

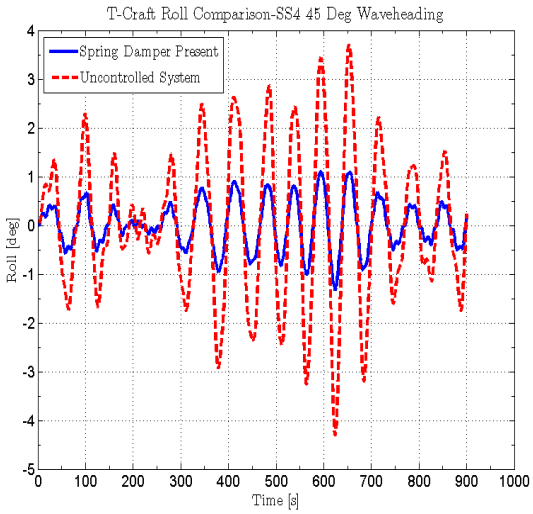

Figure 7.2.4: Roll comparison for controlled vs. uncontrolled system- SS4 WH 45 Deg

These figures illustrate the increase in roll for the wave heading angle of 45°. The passive controller does help reduce the roll; however it cannot eliminate it entirely. As a result, the roll contributes to the ramp pitch angle in cases where the waves approach horizontally. While the controller shows improvement over the uncontrolled case, further work into proper spring selection would yield improved results. At this stage the limitation is the strength of the spring and the implementation onto the physical system, however once more powerful springs become available the stiffness of the spring should be optimized.

Chapter 8 Conclusion

In order to solve the problem of ramp oscillation reduction for the cargo transfer between vessels in moderate sea states, the system was modeled in multiple manners. The first consisted of semi cylinder monuhulls modeled in Matlab. The decoupled equations of motions were used to formulate the system in SimMechanics using springs and dampers. Extremum seeking was used to optimize the ramp length and wave heading angle to reduce the ramp oscillation with success.

The second model was created using the wave seakeeping program, AEGIR, to calculate the hydrodynamic forces of each vessel. A Matlab script was used to communicate with AEGIR and use the hydrodynamic forces while incorporating derived air cushion forces in the systems equations of motion. A backstepping controller was used to regulate the air flow into the air cushion to stabilize the heave and reduce the pitch angle in the ramp. Additionally, a torsion spring and damper were tested on the ramp to investigate the effects on the pitch angle. In each instance, significant reduction in ramp oscillation was observed.

The current phase utilizes a much more advanced version of the T-Craft developed by Navatek and Applied Physical Sciences. The model incorporates the deformability of the air cushion bag and finger system while also using a more advanced fluid model that captures the spatial and temporal variation in pressure throughout the air cushion. This model will be tested with a disturbance rejection algorithm on the unknown plant with adaptive features to solve unknown system parameters.

Bibliography

[1] Bell, Theodore W. "Public Comment on Draft Guidelines and Notices for Passenger Vessels." *United States Access Board*. 13 Nov. 2006. Web. 09 Dec. 2010. <http://www.access-board.gov/pvaac/comments-rev/bell.htm>.

[2] Biran, Adrian. *Ship Hydrostatics and Stability*. Amsterdam: Butterworth-Heinemann, 2003.

[3] "Waterplane Area: Information from Answers.com." *Answers.com: Combined with Free Online Dictionary, Thesaurus, and Encyclopedias*. 8 Dec. 2010. Web. 09 Dec. 2010. <http://www.answers.com/topic/waterplane-area>.

[4] Fossen, Thor I. *Guidance and Control of Ocean Vehicles*. Chichester: Wiley, 1994.

[5] Webster Online. "Dictionary - Definition of Metacentric Height." *Webster's Online Dictionary - with Multilingual Thesaurus Translation*. 8 Dec. 2010. Web. 09 Dec. 2010. <http://www.websters-online-dictionary.com/definitions/metacentric height?cx=partner-pub-0939450753529744:v0qd01-tdlq&cof=FORID:9&ie=UTF-8&q=metacentric height&sa=Search#937>.

[6] Oonk, Stephen H., "Wave-Induced Motion of Ramp-Interconnected Craft", (MS thesis, University of California San Diego, 2008).

[7] Sælid, Steinar, and Nils A. Jenssen. "Adaptive Ship Autopilot with Wave Filter." *Modeling, Identification and Control: A Norwegian Research Bulletin* 4.1 (1983): 33-45.

[8] Ariyur, Kartik B., and Miroslav Krstić. *Real Time Optimization by Extremum Seeking Control*. Hoboken, NJ: Wiley Interscience, 2003.

[9] Farin, Gerald E. *Curves and Surfaces for Computer-aided Geometric Design: a Practical Guide*. San Diego: Academic, 1997

[10] Yun, Liang, and Alan Bliault. *Theory and Design of Air Cushion Craft*. London: Arnold, 2000

[11] Munson, Bruce Roy, Donald F. Young, and T. H. Okiishi. *Fundamentals of Fluid Mechanics*. New York: Wiley, 1994.

[12] Rosenthal, Kring, Milewski, Petersen, Peltzer. "Simulations of a refueling operation of two unmanned surface vehicles." In Proceedings. *Second International Conference on Grand Challenges in Modeling and Simulation.* Istanbul, Turkey. 2009.

[13] Gupta, Kiran C. *Classical Mechanics of Particles and Rigid Bodies*. New York: Wiley, 1988.

[14] Pierson, Willard J., and Lionel Moskowitz. "A Proposed Spectral Form for Fully Developed Wind Seas Based on the Similarity Theory of S. A. Kitaigorodskii." *Journal of Geophysical Research* 69.24 (1964): 5181-190

[15] "Sea State Definition Table." *SyQwest Incorporated, Echo Sounders, Chirp Profilers,Thermal Display Units & More...* Web. 09 Dec. 2010. <http://www.syqwestinc.com/support/Sea State Table.htm>.

[16] Krstić, Miroslav, Ioannis Kanellakopoulos, and Petar V. Kokotović. *Nonlinear and Adaptive Control Design*. New York: Wiley, 1995.

[17] Khalil, Hassan K. *Nonlinear Systems*. Upper Saddle River, NJ: Prentice Hall, 2002.